Department of Applied Physics

Interface Dynamics in Two-Phase Flows with Diffuse Interface Methods

Teemu Laurila

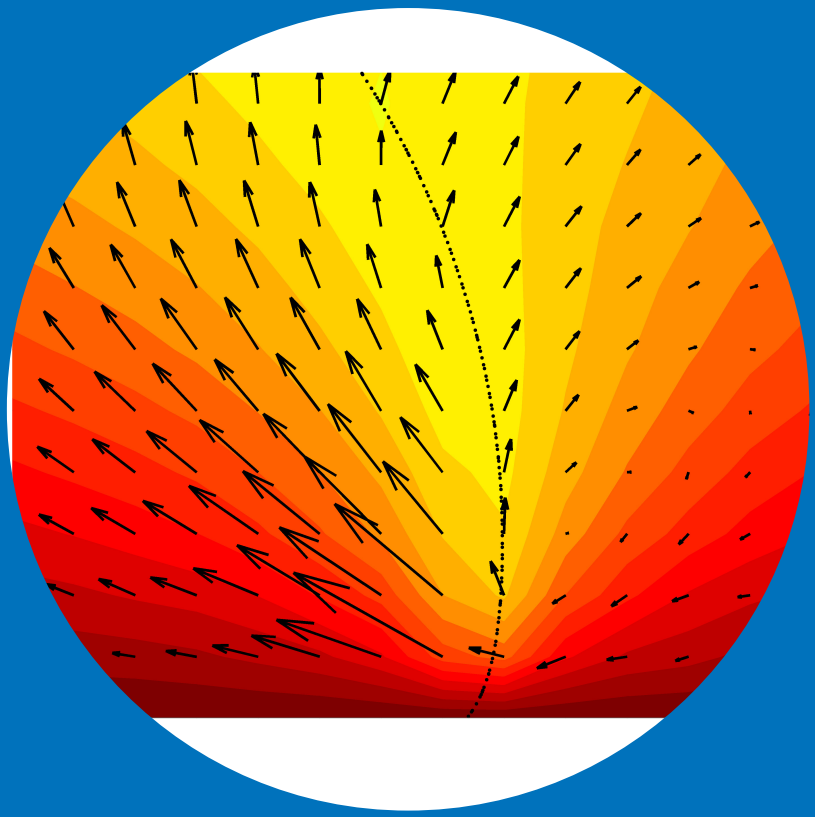

Aalto University

DOCTORAL DISSERTATIONS

Aalto University publication series
DOCTORAL DISSERTATIONS 141/2011

Interface Dynamics in Two-Phase Flows with Diffuse Interface Methods

Teemu Laurila

Doctoral dissertation for the degree of Doctor of Science in Technology to be presented with due permission of the School of Science for public examination and debate in Auditorium E at the Aalto University School of Science (Espoo, Finland) on the 9th of December 2011 at noon.

Aalto University
School of Science
Department of Applied Physics
Multiscale Statistical Physics

Supervisor
Prof. Tapio Ala-Nissilä

Preliminary examiners
Prof. Rodolfo Cuerno, Universidad Carlos III de Madrid, Spain
Prof. John Lowengrub, University of California, Irvine, United States of America

Opponent
Prof. Colin Denniston, University of Western Ontario, Canada

Aalto University publication series
DOCTORAL DISSERTATIONS 141/2011

ISBN 978-952-60-4432-3 (printed)
ISBN 978-952-60-4433-0 (pdf)
ISSN-L 1799-4934
ISSN 1799-4934 (printed)
ISSN 1799-4942 (pdf)

Unigrafia Oy
Helsinki 2011

Finland

The dissertation can be read at http://lib.tkk.fi/Diss/

Publication orders (printed book):
teemu.laurila@aalto.fi

441 697
Printed matter

Aalto University

Abstract

Aalto University, P.O. Box 11000, FI-00076 Aalto www.aalto.fi

Author
Teemu Laurila

Name of the doctoral dissertation
Interface Dynamics in Two-Phase Flows with Diffuse Interface Methods

Publisher School of Sciencce

Unit Deparment of Applied Physics

Series Aalto University publication series DOCTORAL DISSERTATIONS 141/2011

Field of research Engineering Physics, Theoretical and Computational Physics

Manuscript submitted 3 October 2011 **Manuscript revised** 21 November 2011

Date of the defence 9 December 2011 **Language** English

☐ **Monograph** ☒ **Article dissertation (summary + original articles)**

Abstract

Diffuse interface methods are an approach to modeling dynamic multiphase systems. The method allows keeping track of domains of phases and assign physical tension to interfaces in between. In this thesis, two diffuse interface methods are applied to study two different kinds of problems. One is a coarse phase field model of slow dynamics on large scales, and the other a hydrodynamics model of fast dynamics on microscopic scales.

The basis of the phase field model is slow flow of mass on large scales. The model was considered in relation to the experimental Hele-Shaw cell setup. We studied statistics of a propagating interface as it undergoes kinetic roughening due to disorder. Good match was found between the models and the Hele-Shaw setup, but results from both the models and the experiments suggest against a universality class these minimal model systems would potentially represent.

A model of thermal hydrodynamics to study boiling at the microscale was also considered. A method that enables imposing a constant external pressure to the system was developed. The major component of the method is a novel open boundary condition. We verify the method with numerical test cases, and observe the microscale dynamics of nucleate boiling and film boiling under constant pressure. We find a complex flow pattern at the three phase contact line of a growing bubble, which is consistent with the vapor recoil theory of boiling crisis.

Keywords Diffuse Inteface, Phase Field, Two-Phase Flows, Kinetic Roughening, Boiling

ISBN (printed) 978-952-60-4432-3 **ISBN (pdf)** 978-952-60-4433-0

ISSN-L 1799-4934 **ISSN (printed)** 1799-4934 **ISSN (pdf)** 1799-4942

Location of publisher Espoo **Location of printing** Helsinki **Year** 2011

Pages 121 **The dissertation can be read at** http://lib.tkk.fi/Diss/

A! Aalto-yliopisto

Tiivistelmä

Aalto-yliopisto, PL 11000, 00076 Aalto www.aalto.fi

Tekijä
Teemu Laurila

Väitöskirjan nimi
Kaksifaasivirtauksien rajapintadynamiikkaa diffuusin rajapinnan menetelmällä

Julkaisija Perustieteiden korkeakoulu

Yksikkö Teknillisen fysiikan laitos

Sarja Aalto University publication series DOCTORAL DISSERTATIONS 141/2011

Tutkimusala Teknillinen fysiikka, teoreettinen ja laskennallinen fysiikka

Käsikirjoituksen pvm 03.10.2011 **Korjatun käsikirjoituksen pvm** 21.11.2011

Väitöspäivä 09.12.2011 **Kieli** Englanti

☐ **Monografia** ☒ **Yhdistelmäväitöskirja (yhteenveto-osa + erillisartikkelit)**

Tiivistelmä

Diffuusi rajapinnan menetelmillä mallinnetaan materiaaleja ja virtauksia joissa eri alueet voivat olla eri faasissa. Tällä menetelmällä faasien välinen fysikaalinen pintajännitys tulee helposti sisällytettyä rajapintojen monimutkaiseenkin liikkeeseen. Tässä väitöskirjassa kahdella diffuusin rajapinnan menetelmällä tutkittiin kahden eri tyypin ongelmia. Toinen on faasikenttämalli suurten mittaskaalojen hitaaseen dynamiikkaan, ja toinen neste- ja lämpödynaaminen malli nopeaan dynamiikkaan mikroskoopisella skaalalla.

Faasikenttämallin pohjana on hidas massavuo suurella skaalalla. Kokeellinen vastine on n.k. Hele-Shaw koejärjestely. Tutkimme etenevän rajapinnan kineettistä karheutumista sen kohdatessa taustaa joka vaikuttaa siihen satunnaisesti. Laskennalliset ja teoreettiset tuloksemme vastaavat hyvin Hele-Shaw kokeen tuloksia, mutta tulokset eivät tue näkemystä, että näiden minimaalimallien edustama mahdollinen universaalisuusluokka kineettisessä karheutumisessa olisi olemassa.

Tässä väitöskirjassa kehitämme myös keihumisen mallinnukseen sopivaa neste- ja lämpödynaamistä mallia, joka toimii pienissä mittaskaaloissa. Kehitimme menetelmän, jolla voidaan tutkia kiehumista ulkoisen paineen ollessa vakio. Menetelmän päätulos on uusi reunaehto numeeriseen laskentaan. Varmennamme menetelmän fysikaalisuuden useilla testitapauksilla, and käytämme mallia havaitsemaan mikroskaalan lämpö- ja nestedynamiikkaa kun kiehuminen tapahtuu kuplana ja kun se tapahtuu kaasukerroksena. Kuplan kasvaessa kuumalla pinnalla havaitsemme monimutkaisen virtauskuvion, joka on yhdenmukainen kiehumisnopeuden ylärajaa määräävän kaasurekyyli -teorian (vapor recoil) kanssa.

Avainsanat Diffuusi rajapinta, Faasikenttä, Kaksifaasivirtaus, Kineettinen karheneminen, Kiehuminen

ISBN (painettu) 978-952-60-4432-3 **ISBN (pdf)** 978-952-60-4433-0

ISSN-L 1799-4934 **ISSN (painettu)** 1799-4934 **ISSN (pdf)** 1799-4942

Julkaisupaikka Espoo **Painopaikka** Helsinki **Vuosi** 2011

Sivumäärä 121 **Luettavissa verkossa osoitteessa** http://lib.tkk.fi/Diss/

Preface

The work presented in this Thesis has been carried out in Multiscale Statistical Physics group of Aalto University School of Science. Crucial support has been provided by Academy of Finland's Center of Excellence COMP, Fortum Foundation and CSC IT Center for Science.

Foremost I would like to thank my supervisor and mentor professor Tapio Ala-Nissilä for the opportunity he has provided me via the years I have had the pleasure of working in his research group. Tapio has always been supportive of new ideas, and he has put forward not only his knowledge but his contact network of collaborators and visiting scientists for us students. I feel I have had the priviledge to spend these years in an instructive and pleasant environment that has taught me to be a scientist standing on my own feet. Not only in the substance of science, but in the human world of it.

In the course of this work I had the pleasure of working with many brilliant and pleasant people. A special gratitude goes out to Dr. Sami Majaniemi, who taught me by example that you only really understand something if you know things one level deeper. I only wish it would be a standard we could all work by, but you might have set that one too high Sami. A fruitful collaboration with Prof. Aurora Hernández-Machado and Dr. Marc Pradas, that let to Publication III here and taught me of the experiments relevant to first part of this Thesis, is remembered with many thanks. The latter part of this work would never have materialized were it not for a gratefully appreciated collaboration with M.Sc. Andreas Carlson, Dr. Minh Do Quang and Prof. Gustav Amberg. The types of computational tools they develop have the potential to let theoretical physicists do in months what would otherwise take years - at least they did in my case.

I would not have emerged from the years this work has taken the way

I now am were it not for the community created by my fellow students and researchers in our group, particularly my office mates, Olli, Cristian, Akusti and Santtu. Thank you for the camradery. On that note a special mention certainly goes out to all my friends who are not physicists. What sensibility I have, I owe a lot of it to you. My sanity bids you existential thanks.

Reflecting back on life, the greatest thanks for getting me to this point self-evidently goes to my parents and sister. You have always supported me, in ways too numerous to count, and believed in me no matter what. You have been the most important sounding board to me in life, and given advice not so much in terms of what to do, but what to consider. Last but by no means the least my deepest love and appreciation goes out to Henna. With You by my side life looks bright and full of joy, and little tasks like writing this thesis are a breeze.

Helsinki, November 21, 2011,

Teemu Laurila

Contents

List of Publications

This thesis consists of an overview and of the following publications which are referred to in the text by their Roman numerals.

I T. Laurila, C. Tong, I. Huopaniemi, S. Majaniemi, and T. Ala-Nissila. Dynamics and kinetic roughening of interfacesin two-dimensional forced wetting. *European Physical Journal B*, Volume 46, pages 553-561, September 2005.

II T. Laurila, C. Tong, S. Majaniemi, and T. Ala-Nissila. Interface equations for capillary rise in random environment. *Physical Review E*, Volume 74, page 041601, October 2006.

III T. Laurila, M. Pradas, A. Hernández-Machado, and T. Ala-Nissila. Influence of disorder strength on phase-field models of interfacial growth. *Physical Review E*, 78, page 031603, September 2008.

IV T. Laurila, A. Carlson, M. Do-Quang, T. Ala-Nissila and G. Amberg. Thermo-hydrodynamics of boiling in a van der Waals fluid. *Physical Review E*, submitted, September 29th 2011.

Author's Contribution

Publication I: "Dynamics and kinetic roughening of interfacesin two-dimensional forced wetting"

The author did the theoretical calculations presented, and one-half of the numerical calculations. The author wrote the first draft.

Publication II: "Interface equations for capillary rise in random environment"

The author was involved in all of the theoretical calculations presented in the paper. The idea of and calculations with the fluctuating coordinate system was by the author. The author wrote the first draft.

Publication III: "Influence of disorder strength on phase-field models of interfacial growth"

The author performed one half of the numerical calculations presented in the paper and interpreted the results. The author wrote the first draft.

Publication IV: "Thermo-hydrodynamics of boiling in a van der Waals fluid"

The author was central in developing the methodology presented in the paper, performed most of the numerical calculations, and interpreted the results. The author wrote the first draft.

1. Introduction

Fluids and their flow have always been a part of everyday life. One of the oldest pieces of history of science, and one of it's most famous anecdotes, falls under what we today call fluid mechanics: Archimedes and his "Eureka!" moment upon discovering the law of boyancy. Fluid flow in various situations was one of the things that fascinated Leonardo da Vinci enough for him to conduct the oldest known experiments and surviving observations on the topic. The mathematical foundation for describing the flow of fluids was set by Leonhart Euler, by generalizing to continuum the principles of mechanics laid down by Isaac Newton about a century earlier. Euler's equations, as they are known, describe in terms of fields the conservation of mass, momentum and energy, principles that are certainly among the most important in all of physics. Mathematically Euler's equations were likewise a breakthrough, being among the first partial differential equations.

From Euler's equations three additions bring us to what today could be called the full mathematical description of motion of a fluid. First there is a simple law of heat conduction named after Jean Baptiste Fourier, and empirically found to be extremely accurate. Second, an equation of state is needed to describe the pressure of the fluid as function of density and temperature. This additional equation closes Euler's set of equations, which have one more variable than equations and as such are underdetermined. While closing Euler's conservation equations via an equation of state is sufficient and in principle accurate, empirically obtaining the equations of state for real fluids is time consuming at best, and to do the same via theory by considering the fluid as statistics of its constituent particles is even more insurmountable. Third, one needs to consider the tendency of a fluid in motion to drag along any nearby fluid not moving with the same velocity. This is viscosity, or momentum diffusion, and is the reason why

objects moving in a fluid experience drag, which is absent in Euler's equations. The simplest description of viscosity, and most prevalent to this day is linear response, or Newtonian viscosity, which was studied and put to mathematical form already by Isaac Newton.

While the developments described above have led to a well established mathematical description of a fluid, it is limited to fluid that are made of a single material in one phase. But most flows and fluids in nature are multiphase flows. Multiphase flows are mixtures of materials and/or phases. Examples of simpler multiphase flows include air/water/vapor flows of weather phenomena, waves on water/air surfaces like oceans, and steam/water flows in thermal power plant process cycles. The complex end of multiphase flows would be biological matter, ultimately encompassing us human beings. Understandably a complete description of multiphase flows would be complex to the extreme. It is worth noting that many fluids that are in principle multiphase can be described, with varying degrees of accuracy, as a single effective phase. Fluids miscible at the molecular level, such as water/ethanol mixture at athmosperic conditions, is extremely well described as a single phase system. And single phase approximations of significantly more complex fluids can still be useful, for example measurement of blood viscosity in medical applications. Still there are many other types of flows in nature and technology to which the multiphase nature is crucial, and generally it is describing the multiphase nature that is the limiting factor in the accuracy of a mathematical model of a multiphase flow.

Mathematical models of multiphase flows can be divided in a broad sense to two classes of approaches. Prevalent in engineering applications is the effective many-fluid model. In this approach the phases are considered as overlapping continuum fields, which interpenetrate in volume fractions that evolve in time with the flow. This is in effect several overlapping one fluid equations which couple to each other. The approach makes significant simplifications by averaging over typically complex structures of the multiphase flow, assuming the smaller scale properties to average out at sufficently large scales. Consequently these models tend to be simple to be solved as compared to the full complexity of the flow, but hold little predictive power beyond the specific system and circumstance their empirical parameters are engineered to fit.

A more microscopic modelling approach to a flow composed of several phases is to keep track which part of space is occupied by which phase

and the interfaces in between. If the flow pattern is complex this kind of model becomes extremely demanding on computer resources, but within the limits of computational feasibility such a detailed description can give predictive results. These kind of models start with the diffuse interface gas-liquid description of Van der Waals in the mid 19th century[1], a model that is employed in this thesis. Stefan characterized mathematically the problem of a boundary between two phases and the coupled time evolution of the three: two phases and an interface. With the arrival of the computer age, several types of methods have been developed to solve these problems in various applications. These include front tracking, volume of fluid, lattice-Boltzmann, level-set and phase field methods. The latter is the main topic of this thesis. Phase field methods actually share their core methodology with diffuse interface methods as already formulated by van der Waals. As far as fluids are concerned the phase field and diffuse interface can be considered different names for the same method arising from the communities of materials science and fluid dynamics, respectively.

Fluid flow problems are notoriously difficult to solve, and as a consequence several simplifications to the full descriptions have been made. The most famous and widely used of these are certainly the celebrated Navier-Stokes equations developed in the early 19th century [2]. The Navier-Stokes description assumes that the flow field is divergence-free, or incompressible, and is widely applicable in single phase flow. A measure of the mathematical issues of solving flow problems is showcased by the million-dollar prize posted for showing that a unique solution to the Navier-Stokes simplification of single-phase fluid flow even exists [3].

With multiphase flow incompressiblity is much less applicable [4]. Contemporary to Navier and Stokes, a more drastic approximation was made by Henry Darcy to study groundwater flow, which involves water, air and soil. What is now known as Darcy's law assumes that pressure difference relates to flow velocity, as opposed to acceleration as Newton's second law states. This means that Darcy flow decribes the equilibrium state of flow driven by a pressure gradient and subject to friction. The Newtonian anologue of Darcy flow is the terminal velocity of an object. The assumption is valid when the flow is slow and friction is high, that is on time scales larger than the time it takes to reach the terminal velocity. By ignoring advective properties, Darcy flow importantly avoids the mathematical and numerical issues that makes solving the Navier-Stokes

equations so difficult. The simplicity of modeling with Darcy flow has led to it being used today in a wide variety of engineering applications [4, 5].

In the latter part of the 19th century an important experimental insight to Darcy flows was made by Henry Hele-Shaw. Forcing a flow between a narrow gap between two parallel plates, Hele-Shaw's setup simplified the flow, and by using glass plates the flow is easy to study. This setup is now known as the Hele-Shaw cell, and in addition to approximating various flow problems it has gained new popularity with the emergence of microfluidics. [4, 9].

1.1 Hele-Shaw flows and kinetic roughening

Within the last 20 years, much interest has been placed on dynamics of moving interfaces in a more general context of nonequilibrium statistical physics, particularly when the interface is subject to disorder or noise. The morphologies of rough interfaces evolving under the effect of disorder and noise described by fractals and universality[6, 7, 8]. The Hele-Shaw cell setup, with the glass plates roughened to create disorder, was found to be a useful and relatively simple experimental realization in search of universality classes of interface roughening [10, 11, 12, 13]. A crucial factor in terms of a potential universality class of rough Hele-Shaw fronts is that the fluid obeys a conservation law of mass, meaning that expanding a front somewhere takes that fluid mass away from somewhere else. Likewise, disorder must be in fluxes of mass since mass can't spontaneously appear and disappear anywhere - not even if on average the changes would even out to zero.

To model kinetic roughening under a mass conservation law, a phase field model has been deviced that includes the essential and minimal physics. In addition to the conservation law this means a force driving the propagation, surface tension of the interface, and disorder. A generalized phase field model of the type developed by Cahn and Hilliard in the 1950s to microscopically model solidification fronts [14] was found to fit the purpose [15]. The model is know as Model B in the classification scheme of Hohenberg and Halperin [16]. Results from the models were primarily compared with imbibition experiments such as paper wetting [5], which would also fall within the same universality class as rough interfaces in a Hele-Shaw cell.

Simplicity of the generalized Cahn-Hilliard model allows to solve for the dynamics of the roughening interface in terms of the interface itself, sidestepping the bulk. The result is a non-local time evolution equation for the interface, but considered linearized in terms of perturbation theory, it's Fourier space representation is local and quite easily solved numerically.[17] This method we call projection for its ability to project the bulk dynamics to effective terms on the interface evolution equation and it is a central topic of the first part of this Thesis [18, 19, 20]. An interesting property of the projection method is that the effective noise as seen at the interface level can be studied. This effective noise, arising from uncorrelated disorder in the bulk, explicitly shows how the assumption of uncorrelated disorder breaks down when looking at dynamics of the system in terms of projected variables, i.e. with a coarse-grained model.

1.2 Fully hydrodynamic gas-liquid flows, boiling, and boiling crisis

Returning to cases where the full advective properties of fluid low are important, the single-component gas-liquid flow of water and its vapor is a relatively simple multiphase flow with plenty of engineering applications. In heat transfer where boiling water is arguably the most efficient and economic way to transfer heat in devices sizing from microns to industrial scales [4, 9]. The process of boiling as it's commonly observed in the kitchen is known as nucleate boiling, a steady trail of bubbles emerging from a heated surface, and the surface and surrounding fluid is kept very close to the boiling point by formation of gas and thus heat being absorbed into latent heat. Nucleate boiling is a very efficient mode of heat transfer but if the heat throughput is high enough, a continuous gas layer will form at the heated surface instead drastically reducing heat transfer.[21, 22] The reduced heat transfer limits maximum capacity of high-throughput heat exchangers, doubly so because a good safety margin is needed to keep film boiling from happening - the suddenly reduced transfer rate can translate to temperature increases that melt the equipment. This transfer between nucleate and film boiling is called the boiling crisis.

During the past decade a theory to explain how the boiling crisis is formed has been put forth by Nikolayev and co-workers.[23, 24, 25] The vapor recoil hypothesis, as it's known, explains the onset of the transi-

tion from nucleate to film boiling by a single bubble on the hot surface starting to spread out flat along the surface when the heat throughput is high enough, as opposed to growing approximately spherically. Boyancy, because it scales with volume, will make a spherical bubble detach from the surface when it grows large enough, leading to nucleate boiling, but this won't happen if the bubble remains essentially two dimensional near the hot wall.

Crucial to how boiling happens at the microscopic scale is the three-phase gas-liquid-solid contact line, where a bubble is "anchored" on the hot surface it boils on. Almost all boiling happens in the small region surrounding this "foot" of the growing gas bubble, since that's where the gas-liquid phase boundary meets the heat source of the hot surface. Consequently, the gas that gets generated at the contact line must move away and must do so with higher velocity the higher the boiling rate, which is determined by heat throughput. The vapor recoil effect is the force the change in gas momentum imposes on the gas-liquid interface near the contact line due to Newton's third law. While the qualitative picture is theoretically sound, flow profiles at the contact line as boiling happens aren't known either experimentally or by simulation.

From a modeling and simulational point of view, a number of factors make the vapor recoil a relatively attractive problem to tackle, which in the framework of multiphase flows with full fluid dynamics means not completely unfeasible. First, a single bubble is certainly much easier to simulate accurately than collective bubble behavior. Second, the vapor recoil happens when the bubble at the hot surface is still relatively small, as the question is whether the bubble starts growing along the surface as opposed to spherically. Finally, the effect only involves liquid and its vapor and thus the multiphase character is relatively simple.

The central idea in the the original gas-liquid theory of Van der Waals [1] is that the equation of state decribes two phases as function of density, namely a low-density gas phase and a high-density liquid phase. Surface tension is obtained by an energy cost that is attributed to density gradients, which are naturally present when there is a gas-liquid phase boundary. Not long after Van der Waals Korteweg[26] formulated the gradient energy cost in terms of a pressure tensor. When both density and temperature gradients are present, the tensor Korteweg formulated is not sufficient. Mixing temperature and density gradients in such a manner that the resulting forces are reversible, that is isentropic, is the addition

to Korteweg's formulation that leads us to modern diffuse interface methods of gas-liquid dynamics. There are two ways to achieve this, one by Anderson *et al.*[27], and a more recent one by Onuki *et al.*[28].

Only recently, with increasing computing power available, applying diffuse interface hydrodynamics simulations to problems of experimental and practical interest has become feasible.[30, 31, 32] In the last part of this thesis we will apply the diffuse interface thermal hydrodynamics to the vapor recoil problem. To this end we develop and verify a novel boundary condition for the model that allows us to study boiling under constant external pressure.

Computationally the biggest problem of the diffuse interface method is that the theory predicts the width of the interfacial region where density changes from gas to liquid, given the macroscopic properties of equation of state and surface tension. This wouldn't otherwise be a problem, but the widths in question are in the nanometer scale unless we are very close to the gas-liquid critical point, which is not practical for water. The bubbles we would prefer to study, however, extend well into the millimeter scale. The method requires that the interface is resolved with a few nodes on a computational discretization grid, so a problematic separation of length scales is present.

Length scale separation can be numerically alleviated, although not removed, by adaptive mesh refinement, which is a standard tool in modern finite element methods (FEM). Easily applied adaptivity[33] is one of the reasons we apply the femLego symbolic FEM toolbox[34], the other being that the toolbox allows us to carefully set the time integration scheme, while allowing automating space discretization. Time integration for compressible flows is another tricky computational point, to which we choose the characteristics-based-split method of Nithiarasu *et al.*[36, 35].

With our implementation of the diffuse interface thermohydrodynamics we achieve what are to our knowledge the first simulational results showing the vapor recoil mechanism including the full hydrodynamic fields around the contact line as boiling under constant external pressure happens. While these simulations are not yet directly applicable to the engineering problem of boiling crisis, they are a step in understanding what happens in general. They also constitute a step towards determining whether the vapor recoil theory accurately describes what happens in reality, especially as direct comparisons to critical boiling experiments[25, 22] becomes possible.

Generalization of the experience of this author as a computational physicist working with the femLego toolbox is one that is worth mentioning. After having programmed everything from scratch in the first, Hele-Shaw flow, part of the work in this thesis, the experience of using a toolbox where almost all of the work of making computational grids is automated was a positive one. An interface such as the femLego toolbox allows both the physicist and the computational specialist to work in their own areas of expertise, greatly increasing efficiency greatly. In the humble opinion of this author, it will be a way of the future in making computational science. Not only a positive development, but a necessary one as the field of computational physics grows, and the next generation must be allowed build on top of past knowledge without the physicist re-inventing every numerical wheel.

2. Hele-Shaw Flows and Phase Field Models

The Hele-Shaw cell has been proposed as a model system for a class of kinetic roughening under two complicating conditions compared to the most simple Family-Vicsek scaling[7]: The roughening is caused by quenched, spatial disorder, as opposed to time-dependent thermal noise, and a conservation law is present in the propagating medium.[37, 10, 11] An experimental setup to study fluid invasion into a Hele-Shaw cell containing disorder manufactured to desired specifications is presented in Fig. 2.1. In the experiment one tracks the moving interface described by a height function $h(x,t)$. The statistical properties of $h(x,t)$, averaged across different realizations of disorder in the Hele-Shaw cell walls, constitute the potential universality class of kinetic roughening.

2.1 Characterizing Rough Interfaces: Power-Law Scaling

The most important or at least the most widely-used statistical quatity in describing the roughness of a moving interface $h(x,t)$, whether one or two dimensional, is the interface width

$$w_L(t) = \left(\langle \, \overline{(h(x,t) - \overline{h(x,t)})^2} \, \rangle \right)^{1/2}, \tag{2.1}$$

where the overbar denotes average over x taken over length L, and square brackets are ensemble average of different disorder realizations. In the Family-Vicsek scaling picture the width increases as a power-law in time until a saturation time is reached when correlations reach the size we observe the system at. After the saturation time the width is a constant that increases as power-law in the width of the system. This is expressed as

$$w_L(t) \propto \quad t^{\beta} \quad , \; t < t_s \tag{2.2}$$

$$w_L(t) \propto \quad L^{\chi} \quad , \; t > t_s, \tag{2.3}$$

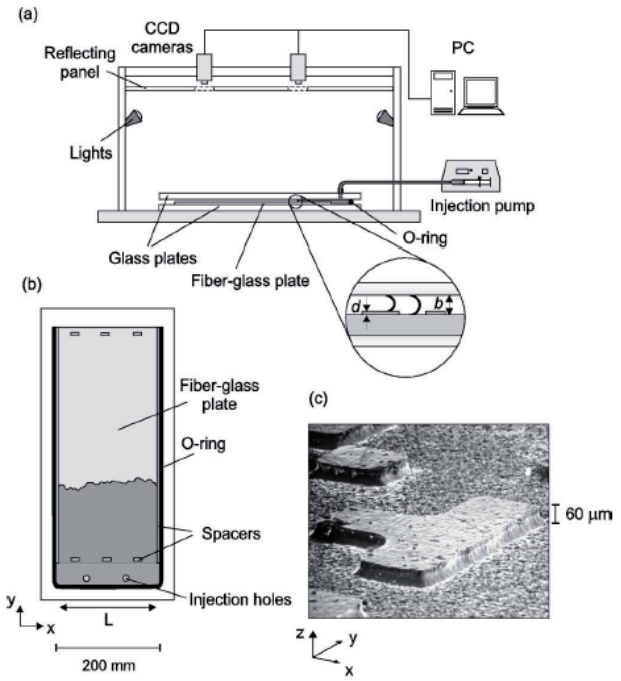

Figure 2.1. (a)-(b) A schematic representation of the Hele-Shaw cell experiment with controlled disorder. Image of the disordered glass plate is shown in cc) To study flow driven by a constant pressure gradient, as opposed to constant liquid influx, the injection pump can be replaced by a reservoir with liquid suface at constant height above the horizontal cell. Experiments conducted by Soriano *et al.*, image from [10].

where t_s is saturation time, and the exponents β and χ are the growth and roughness exponents. Finally the saturation time must depend on L as $t_s \propto L^z$, where z is called the dynamic exponent. If this simple scaling ansatz holds, then equating widths at saturation time gives $chi = z\beta$.

Qualitatively, Family-Vicsek scaling then states that interface roughness will grow, with power-law exponent β, until correlations along the interface reach the size we're observing the system at. The correlations along the interface are related to its undulations in the perpendicular direction, the width, by the power-law exponent χ. Roughness exponent χ means that the interface will have the same properties if we change the scale of observation by factor a_x in the direction along the interface, and by factor $a_z = a_x^\chi$ in the perpendicular direction. This property is called self-affinity, and it is a generalization of self-similarity of "simple" fractals where $\chi = 1$, meaning all directions are equal.[7] Physically, self-affinity arises when an action breaks the symmetry between the directions along and perpendicular to the interface. For example, a force driving the interface forward usually does this.

In this thesis, we will observe two types of deviations from the Family-Vicsek scaling picture, attributed to the effects of the conservation law in fluid and the quenched disorder present in the Hele-Shaw cell. First, a super-rough interface is found, where $\chi > 1$. Since an infinitely more serrated interface at larger scales, which $\chi > 1$ impliesm is unphysical, an upper crossover scale away from super-rough behavior is expected. It means that in scales smaller than the crossover scale ξ_x, we find Family-Vicsek scaling, but if we look at larger scales than ξ_x, then the roughness will no longer increase and the system is no longer self-affine:

$$w_L(t > t_s) \sim \begin{cases} L^\chi & \text{for} \quad L < \xi_x; \\ \chi_x^\chi & \text{for} \quad L > \chi_x, \end{cases} \tag{2.4}$$

We predict the crossover scale ξ_x using the projection method for a Hele-Shaw interface driven by constant flux, previously this has been done for driving via constant pressure [38], and verify its existence via numerical simulations.[18] The origin of the crossover ξ_x is the mass conservation law, which prevents undulations from growing beyond certain level because they can't be fed by the incoming flux. For this reason ξ_x depends on the speed with which the interface advances.

A useful property in statistical analysis of an interface is the strucure

factor, based on the Fourier spectrum

$$\tilde{h}(k,t) = \frac{1}{L}\int \mathrm{d}x e^{ikx} h(x,t), \tag{2.5}$$

where the integral reaches over the entire system, not just a chosen observation window L. The structure factor $S(k,t)$ is the disorder average of the absolute value of the (complex) spectral component k,

$$S(k,t) = \langle \tilde{h}(k,t)\tilde{h}(-k,t)\rangle. \tag{2.6}$$

Defining the spectral roughness exponent χ_s, the structure factor follows the scaling form

$$S(k,t) = k^{-(2\chi+1)} s_A(kt^{1/z}), \tag{2.7}$$

where the scaling function has the general form

$$s_A(u) \sim \begin{cases} u^{2(\chi-\chi_s)} & \text{for} \quad u >> 1; \\ u^{2\chi+1} & \text{for} \quad u << 1. \end{cases} \tag{2.8}$$

The structure factor is useful in determining the roughness exponent for Family-Vicsek scaling as well as the super-rough scaling. Under conditions that are valid for the Hele-Shaw flow, including the super-rough scaling with cutoff ξ_x, we find scaling with $\chi_s = \chi$. In a borderline case for high disorder strength in a numerical model we observe more complex intrinsic anomalous scaling[39], where $\chi_s \neq \chi$. Special property of intrinsic anomalous scaling is that local properties of the interface change until the largest scale has saturated, i.e. ξ_x is reached in correlations in our case. Time dependence of the structure factor in the long time limit is a tell-tale sign of the anomalous scaling.

2.1.1 Phase-Field Model

The phase-field model called Model B in the classification scheme of Hohenberg and Halperin [16] is a coarse-grained model that captures the propagating front and the conservation law between the front and the boundary the driving is imposed on. It was developed for modeling solidification by Cahn and coworkers [14], and adapted for modeling Hele-Shaw cells and imbibition in general by Dubé and collaborators[15]. Fluid invasion is modeled by a phase field ϕ, which has the value $\phi = 1$ in the wet phase and $\phi = -1$ in the dry. A gradient free energy term gives surface tension between wet and dry. The model is diffusive propagation of the wetting, with a flux given by Farcy flow, or equivalently Fick's law, with

mobility M:

$$\partial_t \phi(\mathbf{x},t) = \nabla \cdot (M \nabla \mu(\mathbf{x},t)), \tag{2.9}$$

where the chemical potential gradient (analoguous to pressure gradient in Darcy flow), is given by a Ginzburg-Landau free energy:

$$\mu(\mathbf{x},t) = \frac{\delta \mathcal{F}[\phi(\mathbf{x},t)]}{\delta \phi}; \tag{2.10}$$

$$\mathcal{F}[\phi(\mathbf{x},t)] = \frac{1}{2}(\nabla \phi(\mathbf{x},t))^2 - \phi^2/2 + \phi^4/4 - \alpha(\mathbf{x})\phi(\mathbf{x},t). \tag{2.11}$$

The model is built such that the two minima of the free energy at $\phi = 1$ and $\phi = -1$ can represent any two phases with a mass conservation law between them. Physically this corresponds to phases consisting of two different substances, such as air and water. The phase field separating between the volumes of air and water must be conserved, because under no circumstance can the substances turn into on another.

The phase field equations above have a one dimensional equilibrium solution corresponding to a planar interface between the two stable phases. When the simple Ginzburg-Landay free energy is used, this solution has the exact analytic form

$$\phi_0(u) = \tanh(\frac{u}{\sqrt{2}}), \tag{2.12}$$

where u is the coordinate normal to the planar interface, located at $u = 0$, and boundary conditions are $\{\phi = -1 \text{ at } u \to -\infty\}$ and $\{\phi = 1 \text{ at } u \to \infty\}$. This solution is valid for zero disorder, and thus it is frequently called the zeroth order solution, anticipating a perturbative expansion in disorder and interface fluctuations. Using this solution, it can be shown that the dimensionless surface tension in the model is $\sigma = \int \mathrm{d}u \, (\partial_u \phi_0(u))^2 = \frac{\sqrt{2}}{3} \approx 0.47$.[14] Mapping this to a physical surface tension then sets the dimensionless length scale in our model. If the mobility M is constant, then we can set it to $M = 1$ by setting out dimensionless time scale in the model. However, we also consider a mobility that includes a disorder component:

$$M = 1 + \xi(\mathbf{x}). \tag{2.13}$$

We consider two different types of disorder in the system, modeled by the stochastic variables α and ξ. Chemical potential disorder $\alpha(\mathbf{x})$ sets the wettability of different locations to be different, whereas mobility disorder $\xi(\mathbf{x})$ set a different flux response to the same potential gradient. We consider the stochastic variables to be Gaussian and uncorrelated:

$$\langle \alpha(\mathbf{x}) \rangle = \bar{\alpha} \tag{2.14}$$

$$\langle \alpha(\mathbf{x}) \alpha(\mathbf{x}') \rangle = (\Delta\alpha)^2 \delta(\mathbf{x} - \mathbf{x}'), \tag{2.15}$$

and indentically for ξ. Above $\bar{\alpha}$ is the average and $\Delta\alpha$ is the standard deviation.

With the Hele-Shaw cell experiment in mind, we can set the model for both spontaneous and driven imbibition. In the experiment the spontaneous imbibition is achieved via a fixed hydrostatic pressure between the cell and a reservoir of liquid being driven, whereas driven imbibition is achieved via a pump set to inject liquid with constant volume flux. In the model, spontaneous imbibition is modeled by setting a positive constant $\bar{\alpha} > 0$. Then the boundary condition at wet, driving end is $\mu = \text{const.} = 0$. In driven imbibition there is no spontaneous wetting, $\bar{\alpha} = 0$, and the boundary condition at the driving end is a constant flux $\nabla_n \mu = F$.

With this phase-field model we consider a simpler 2D model, where the model is defined in the plane of the Hele-Shaw cell and disorder is put explicitly into either $\alpha(\mathbf{x})$ or $\xi(\mathbf{x})$. We also consider a full 3D model of the Hele-Shaw cell. Here roughness on the Hele-Shaw cell walls is explicitly included as stochastic location of the boundary condition of the cell wall. Figure 2.2 shows a schematic of boundary conditions in the phase field model and how the chemical potential, phase field, and roughening interfaces look like in the model.

2.1.2 Interface Projection Method

Assuming that the curvature of the wet-dry interface is smaller than the width of the diffuse interface in the phase-field model, we can project the bulk dynamics including the conservation law, to an effective interface model.[17] This projection can be performed identically for the 2D or 3D phase field model, and turns into a 1D interface equation, or a 2D meniscus equation, respectively. Formally the procedure is the same regardless of dimensionality. The difference lies in the Green's function that we use to invert the Laplacian in the phase field equation (2.9).

The projection method consists of seven steps. Here we will overview it in general, more details are presented in Publication I and Publication II of this thesis, as well as in references[14, 17]. To perform the projection we first turn the phase field equation (2.9) into the corresponding integro-differential equation using the proper Green's function for the Laplacean

$$\nabla^2 G(x, y|x', y') = \delta(x - x')\delta(y - y'), \tag{2.16}$$

taking into account the boundary conditions, which physically correspond to spontenous or driven propagation. For half-space geometry, the Green's

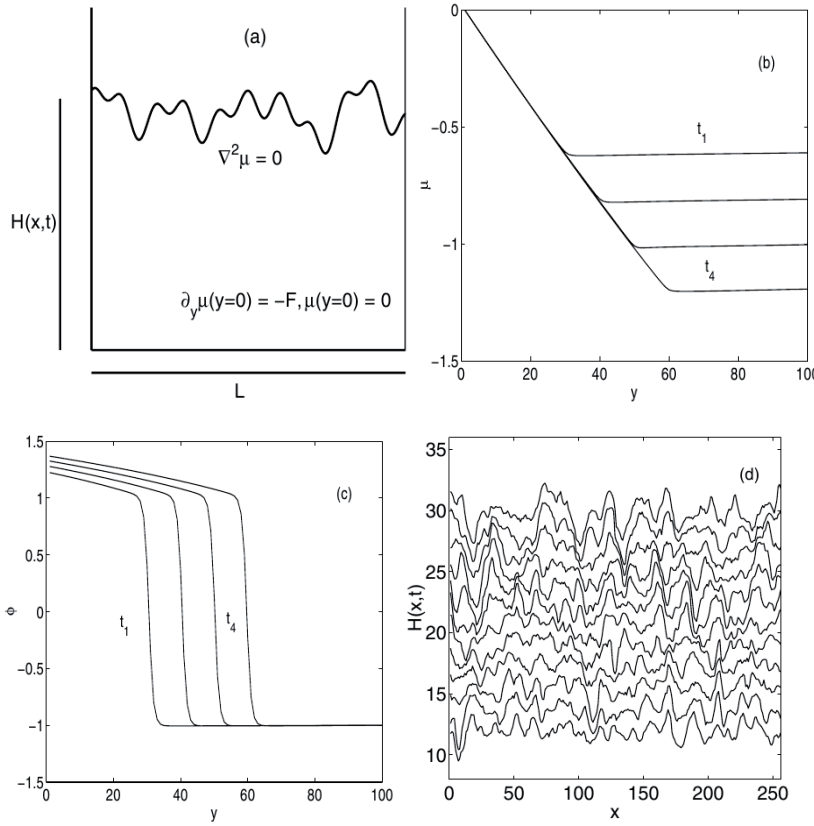

Figure 2.2. (a) A schematic geometry and setup of the phase field model. The height of the front is described by a single-valued function $h(x,t)$, and the driven boundary condition at the reservoir at $y = 0$ is described by a constant gradient of the chemical potential. (b) The profile of the chemical potential $\mu(x,y)$ along the y axis at successive time steps $t_1 < t_2 ... < t_4$. (c) The profile of the density field $\phi(x,y)$ along the y axis at successive time steps corresponding to (b). Note that due to the conservation law these profiles have a finite slope in the wet region of the medium. (d) A set of typical rough front configurations of a rising interface $h(x,t)$ taken at equal time intervals.

functions are

$$G(x,y|x',y') = \frac{1}{4\pi}\ln\left[((x-x')^2+(y-y')^2)((x-x')^2+(y+y')^2)^{\pm 1}\right], \tag{2.17}$$

where the upper plus sign corresponds to driven and the lower minus to spontaneous propagation, or Dirichlet and Neumann boundary conditions. This Green's function is obtained by the image charge method. Assuming no mobility disorder, $\xi = 0$, the phase field equation in integro-differential form reads

$$\int_V \mathrm{d}\mathbf{x}' G(\mathbf{x}|\mathbf{x}')\partial_t\phi(\mathbf{x}') = \mu(\mathbf{x}) + \Lambda, \tag{2.18}$$

where Λ is a surface contribution from inhomogenous Neumann boundary condition, which becomes relevant in the case of driven propagation.

As second part of the projection method, we write the integro-differential form in terms of interface coordinates (u,s), where u is normal to the interface and s is along it. Third part is to do the actual projection to the interface with the projection operator obtained from the 0th order solution

$$P[\cdot] = \int \mathrm{d}u\partial_u\phi_0(u)[\cdot]. \tag{2.19}$$

The projection is valid, i.e. does not project out relevant dynamics of the system, if the interface radius of curvature is much larger than the interface width. The projected equation in interfacial coordinates reads

$$\int \mathrm{d}u\partial_u\phi_0 \int \mathrm{d}s'\mathrm{d}u' G\partial_t\phi' = -\sigma\kappa - \int \mathrm{d}u\partial_u\phi_0\alpha + \Lambda, \tag{2.20}$$

where $\kappa = \partial_x^2 H(x,t)$ is the local interface curvature.

The fourth step in the projection is to take the sharp interface limit, assuming that the interface width goes to zero, $\phi_0 \to -1 + 2\Theta(u)$, where Θ is the Heaviside step function, while keeping the surface tension constant. This limit allows us to evaluate the integral in the normal direction above. The fifth step is to transform the resulting interface equation back to Cartesian coordinates using $ds\partial_t u = dx\partial_t H(x,t)$, yielding

$$2\int_{-\infty}^{\infty} \mathrm{d}x'\; G(x,H(x,t)|x',H(x',t))\,\frac{\partial H(x',t)}{\partial t} = \alpha(x,H(x,t)) + \sigma\kappa + \Lambda. \tag{2.21}$$

The projection operation itself is complete with the above non-local interface equation since the equation gives the time evolution of the interface $H(x,t)$ as a function of itself. Solving the complete equation is not possible, though, so two more steps are needed. The sixth step in the method is to linearize the equation in small fluctuations and disorder $H(x,t) = H_0(t) + h(x,t)$. For the zeroth order solution, the motion of the

average interface, depends on the boundary conditions and is the Washburn law for spontaneous propagation, or constant velocity for the driven propagation

$$\partial_t H_0(t) = \begin{cases} \frac{M\bar{\alpha}}{2MH_0(t)} & \text{for spontaneous;} \\ \frac{F}{2} & \text{for driven.} \end{cases} \tag{2.22}$$

The linear order equation for fluctuations is still a non-local integro-differential equation. But since it's linear, it's now by construction a convolution of the Green's function and $h(x,t)$. Because the Fourier transform of a convolution is always local in reciprocal space, the seventh and final step to obtain the linearized interface equation (LIE) from the projection method is Fourier transform. In the case of driven propagation, the Green's function is not square integrable and thus doesn't have a simple Fourier transform. We go around this problem in Publication I of this thesis by performing the discrete Fourier transform in a strip of finite length, and taking the limit after the equation of motion is obtained for the discrete Fourier components. The resulting linear order equations, containing a dispersion relation for fluctuations and an effective noise term, are

$$\dot{h}_k \left(1 \pm e^{-2|k|H_0}\right) = |k| \left(-\dot{H}_0 \, h_k \left(1 \mp e^{-2|k|H_0}\right) - \sigma k^2 h_k + \eta_k(t)\right), \tag{2.23}$$

where the upper signs correspond to driven interface propagation, and lower signs to spontaneous. From the spontaneous case here, Dubé *et al.* predicted the existence of a cross-over scale $\xi_x = 2\pi\sqrt{\frac{\sigma}{\partial_t H_0(t)}}$, and numerically showed that at scales larger than ξ_x the interface is asymptotically flat [15]. In Publication I of this thesis, we showed that this scale remains the same with driven propagation, although the average interface velocity is then constant as opposed to being time dependent.

In Eq.(2.23) the effective disorder term looks deceivingly simple. It is, however, non-local in Fourier space, and in order to numerically solve for it, a back-and-forth Fourier transform is needed every timestep

$$\eta_k(t) \equiv \int dx \; e^{-ikx} \alpha(x, H(x,t)). \tag{2.24}$$

One should note that the term $|k|$ in front of the effective disorder in reciprocal space also means a non-local effect in real space. Thus the conservation law shows manifestly in the effective disorder.

Complications arise to the projection method in the case of the mobility disorder ξ. A more detailed account of the case is given in Publication II of this thesis. The end result is an effective disorder term that differs form the one from α disorder above. The qualitative change in mobility disorder

is that the effective disorder ends up being propotional to $|k|\partial_t H_0(t)$ as opposed to $|k|$.

2.2 Driven Interface Propagation

In Publication I, we numerically intergrated both the 2D phase field model with driven propagation and the LIE derived from it by the projection method. We used chemical potential disorder α and no mobility disorder $\xi = 0$. We compare the results from both, obtaining the cross-over length scale ξ_x as well as the roughness exponent χ and the growth exponent β.

Assuming that the roughening of the interface is follows Family-Vicsek scaling with the crossover length $\xi_\times$ as an upper limit of lateral correlations (instead of the system size L) we can follow Ref. [15] and write a scaling relation as

$$w(t) = \Delta\alpha\xi_\times^\chi \, g\left(\frac{t^\beta}{\xi_\times^{\chi/\beta}}\right), \tag{2.25}$$

where g is a scaling function. In Figure 2.3 we show the interface width obtained from the phase field model, and the data collapse according to Eq. (2.25). If the scaling picture, and the roughness and growth exponents are correct, then data from different parameters should collapse to the scaling function g. Based on when the collapse happens, our best estimates are $\chi = 1.35 \pm 0.05$ and $\beta = 0.50 \pm 0.02$ for the phase field model. The data collapse shows that the interface roughening follows super-rough scaling, i.e. Family-Vicsek with $\chi > 1$, and that ξ_x is the large scale limit, beyond which the interface is asymptotically flat. Similarly for the LIE we obtain $\beta = 0.37 \pm 0.04$ and $\chi = 1.27 \pm 0.05$.

To further verify the scaling picture we show the structure factors from both the phase-field model and LIE on the right hand side of Figure 2.3. The roughness exponent fitted to the scaling form of Eq. (2.8) given by $\chi_s = \chi$, agrees with our results from the width scaling for both the phase field and the LIE.

We note that while the LIE properly reproduces the spatial roughness exponent of the phase-field model, there is a difference in the growth exponent. The exponents obtained from the phase field model are in agreement with Hele-Shaw experiments with roughened cell walls[10, 11].

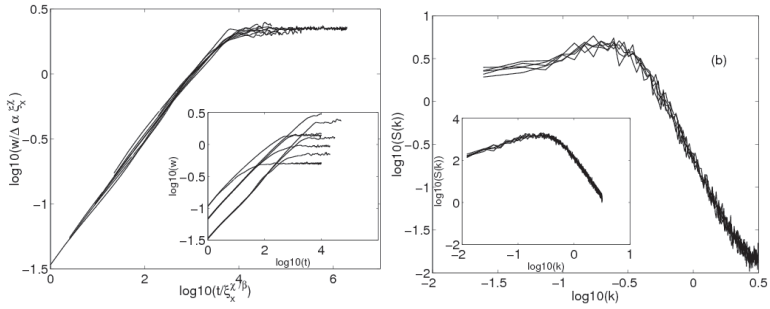

Figure 2.3. Data from driven propagation of wetting front and α disorder. On the left hand side, we show data collapse of the interface width from the phase field model according to the scaling form of Eq. (2.25), for different sets of parameters. Inset shows the raw data. On the right hand side, the structure factor $S(k,t)$ plotted against the wave vector k as obtained from the phase field model. In the inset, the same is plotted for the LIE.

2.3 Meniscus and Contact Line in Hele-Shaw Cell with Fluctuating Wall

The integro-differential form of the phase-field equations central to the projection method led us to the idea that it could be used to describe the Hele-Shaw cell more faithfully than the two-dimensional phase-field model with the disorder input effective in either ξ or α. The Green's function allows us to study the phase-field equations in a 3D geometry where the wall of the cell is explicitly fluctuating, and to obtain effective noise terms for the 2D liquid-air interface, ie. meniscus, and the 1D contact line where the meniscus meets the cell wall. This is all done at the same linearized level of perturbations as the LIE above.

The basis of the fluctuating wall analysis is a coordinate transformation to coordinates where the fluctuating wall, located at $y = \delta Y(x,z)$ where δY is now the stochastic variable, is cast to be straight. The idea is schetched in Figure 2.4. We consider the simplest case of one wall, which means a geometry of one-quarter space in 3D, or two bounding planes. The lower plane at $z = 0$ is the driving boundary condition, whereas the left plane at $y = \delta Y$ is the fluctuating physical wall.

Using the coordinate transformation, the projection method from the 3D phase-field to the 2D meniscus can be performed straightforwardly in the fluctuating coordinates, and transforming back leads to an interface equation where the noise is in the Green's function

$$\int \mathrm{d}x'\mathrm{d}y' \tilde{G}_{3\mathrm{D}}(x,y,H(x,y;t);x',y',H(x',y';t))\frac{\partial H(x',y')}{\partial t} = \sigma_B \kappa, \qquad (2.26)$$

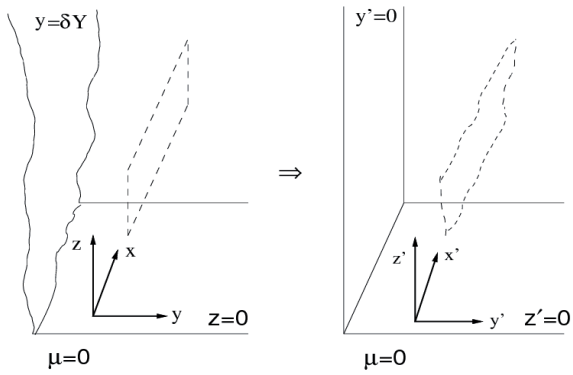

Figure 2.4. A schematic presentation of the curvilinear coordinates used to describe a fluctuating wall. When presented in terms of curvilinear coordinates, the rough wall by definition look straight. However, the shift has introduced a coordinate fluctuation in space, where a previously rectangular object looks curved when presented in terms of the new coordinates. This gives rise to a bulk representation of the fluctuating wall, which can be analyzed more easily than the original boundary condition representation.

where $\tilde{G}_{3\mathrm{D}}$ is the Green's function in the fluctuating coordinates, and considered in detail inPublication II, and the Appendix therein. Linearizing the fluctuations in the Green's function in both δH and $h(x,t)$, we obtain

$$\begin{aligned}\tilde{G}_{3D}(x,y,H(x,y);x',y',H(x',y')) \simeq G_{3D}(x,y,H_0;x',y',H_0)\\ +\delta Y(x,H_0)\partial_y G_{3D}(x,y,H_0;x',y',H_0)+\delta Y(x',H_0)\partial_{y'}G_{3D}(x,y,H_0;x',y',H_0)\\ +h(x,y;t)\partial_z G_{3D}(x,y,z;x',y',H_0)|_{z=H_0}+h(x',y';t)\partial_{z'}G_{3D}(x,y,H_0;x',y',z')|_{z'=H_0},\end{aligned} \tag{2.27}$$

where $\tilde{G}_{3D}$ is the Green's function in the normal Cartesian coordinates. In retrospect this results isn't very surprising because it is obtained by the chain rule and fluctuations in arguments of the Green's function.

After transforming the linearized equation into reciprocal space, we obtain the linearized equation for meniscus fluctuations as

$$\partial_t h(\vec{k},t) = -\frac{k\partial_t H_0(t)\left(1+e^{-2H_0(t)k}\right)+\sigma_B k^3}{\left(1-e^{-2H_0(t)k}\right)}h(\vec{k},t)+k\dot{H}_0\delta Y(\vec{k},H_0). \tag{2.28}$$

In particular, the effective disorder term above is proportional to interface propagation velocity, in accordance with what we obtain for mobility disorder ξ in Publication II.

We analyze the 3D case further by looking at the contact line at the wall in the quarter-space setup. To do this an additional projection mechanism is needed. In analogy to the 1D kink solution normal to the interface we need to link the contact line and the meniscus. If we assume that the

meniscus obtains the form that minimizes surface tension given that the contact line is set, we get what is called the quasi-stationary approximation: $\nabla^2 h(x,y;t) = 0$; $h(x,0,t) = c(x,t)$.

To use the quasi-stationary approximation, we re-write the meniscus equation (2.26) in terms of a free energy functional and Rayleigh dissipation functional:

$$\frac{\delta R_{\mathrm{2D}}[\dot{H}]}{\delta \dot{H}(x,y;t)} = -\frac{\delta F_{\mathrm{2D}}[H]}{\delta H(x,y;t)}. \tag{2.29}$$

The forms of the functionals R_{2D} and F_{2D} are presented in detail in Publication II. Inserting the quasi-stationary approximation into the functional variations, linearizing in fluctuations and noise, and Fourier transforming to reciprocal space yields a linearized equation for the contact line

$$\dot{c}(k_x,t) = -\frac{\frac{3\pi|k_x|\dot{C}_0}{8}\left(1+e^{-2.28|k_x|C_0}\right)+\sigma_B|k_x|^3}{\left(1-e^{-2.28|k_x|C_0}\right)}c(k_x,t) + \frac{3}{2}|k_x|\dot{C}_0\delta Y(k_x,C_0). \tag{2.30}$$

As explained in Publication II this form contains some exponential approximations to integrals that are not exactly solvable in that closed form, but the approximations differs by only a few percent even in worst case scenario as function of all the parameters.

We note that the equation for the contact line fluctuations thus obtained has no qualitative differences to the meniscus equation. This means that if the quasi-stationary approximation is made, meniscus and contact line fluctuations follow similar dispersion relations. This is not surprising given the nature of the quasi-stationary approximation, which assumes that the meniscus and contact line relax to their common minimum surface faster than any other time scale in the system. Setting a finite time scale in between would make the calculation extremely complicated.

2.4 Breakdown of Linearized Fluctuations: Strong Disorder

Above we performed extensive calculations at the level of linearized fluctuations of the interface in the conserved phase-field model. A natural question to ask is when is the small fluctuations assumption valid. In Publication III, we consider two different versions of the two-dimensional phase field model at different disorder strenghts. The goal is to find the limit to the regime of small disorder and to look at what happens to the kinetic roughening in our model when the interface strength is increased.

Experiments on a Hele-Shaw cell with large disorder were performed by Soriano *et al.* [11].

We use the two-dimensional phase-field model with potential disorder α. In addition to the constant mobility model $M = \text{const.}$ considered above, we consider the model of one-sided mobility $M = M_0\theta(\phi)$, $\theta(\phi)$ being the Heaviside step function. Thus the mobility is zero in the phase where $\phi < 0$. The phase field time evolution equation (2.9) remains the same. The one-side model has been considered in terms of kinetic roughening and Hele-Shaw cells by Hernández-Machado *et al.*[40], and the results for low disorder agree with ours with a constant mobility.

The one-side model works when the interface monotonically grows, i.e. the wet $\phi = 1$ phase advances into the dry $\phi = -1$ phase. This means $\partial_t\phi \geq 0$ everywhere. In numerics this means that flow from a node with $\phi > 0$ into a neighboring node with $\phi < 0$ has mobility M_0.

We estimate the strength of the disorder by comparing the free energy of a uniform phase in a area where the disorder is unfavorable to it to the case where the phase is changed to be different from the surroundings in the area to conform to the disorder. The non-uniform phase costs interface energy. Considering a circular area of radius r, the standard deviation of the disorder averaged over the area is $\langle\alpha\rangle_r = \frac{\Delta\alpha\, l_{corr}}{r}$, where l_{corr} is correlation lenght of the disorder, or the same as our numerical grid spacing. The above comes directly by taking the amount of uncorrelated disorder sites in the area, and summing up those as independent random variables.

It is then favorable for the phase field in the area to be different from its surroundings if the surface energy cost is less than the energy gained by conforming to the disorder

$$2\pi r\sigma \leq \pi r^2 \Delta\phi \langle\alpha\rangle_r, \tag{2.31}$$

where the miscibility gap in our model is $\Delta\phi = 2$. Thus, we obtain an estimate for the strong disorder limit as

$$\Delta\alpha \geq \frac{\sigma}{l_{corr}}. \tag{2.32}$$

In our dimensionless units for the phase field with $l_{corr} = \Delta x = 1$, and $\sigma = \sqrt{2}/3$ and thus we obtain an estimate for strong disorder regime as $\Delta\alpha \geq \sigma \approx 0.47$.

One relevant thing to note of the disorder strenght estimate is that it does not depend on the lenght scale r. This means that in the strong

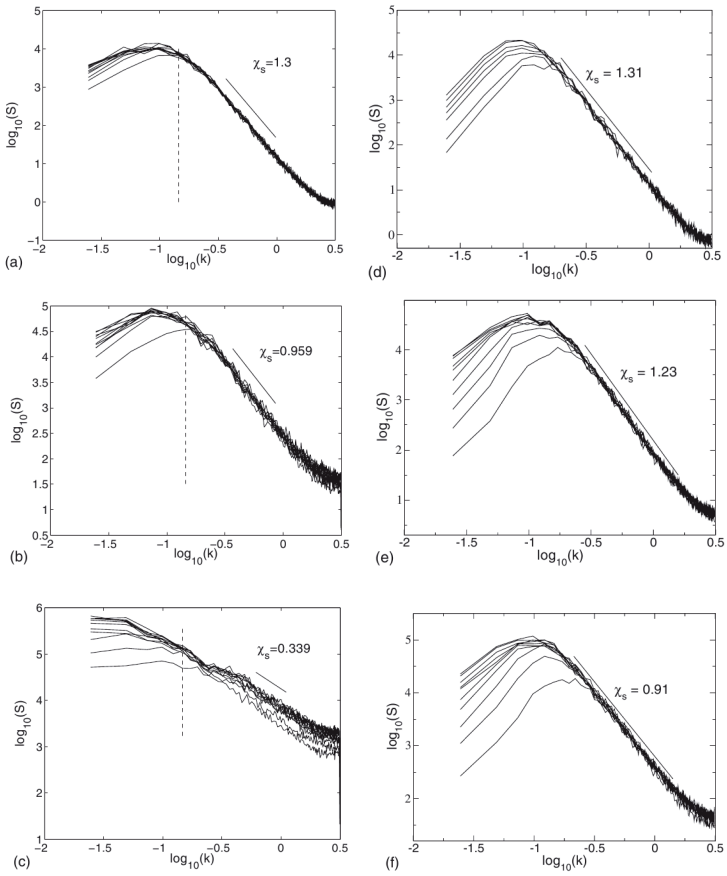

Figure 2.5. Structure factors at ten equidistant time intervals for the two phase field models at different disorder strengths (in dimensionless units). Results from the symmetric and one-sided model are given in the left(a,b,c) and right(d,e,f) panels, respectively. Disorder strengths are varied from up to down as weak ($\sigma = 0.2$), intermediate ($\sigma = 0.5$) and strong ($\sigma = 1$). Fitted roughness exponents are given in the figures, with solid lines corresponding to the fits.

disorder regime, the phase field is expected to form domains of all sizes equally.

The clearest picture of the roughening under different disorder strenghts is given by the spectral roughness exponent χ_s. In Figure 2.5, structure factors are shown for both phase field models at different disorder strenghts. As the disorder is increased, universal super-rough scaling breaks down and the spectral roughness exponent decreases continuously as a function of the disorder.

In Fig. 2.6 the spectral roughness exponent is plotted in both phase field models. In the small fluctuation regime, given roughly by $\Delta\alpha < 0.5\sigma$, a universal scaling picture by super-rough scaling with well determined

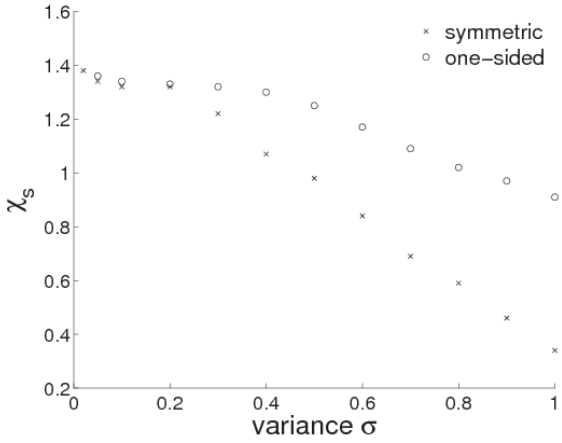

Figure 2.6. Spectral roughness exponent χ_s for both phase field models as a function of the disorder strength.

exponents is found. As disorder is increased beoynd this the models start to behave differently and the roughness exponent depends continuously on disorder in both cases.

At strong disorder the roughness of the interface in the symmetric model is determined by the interface incorporating domains as considered in the disorder strength estimate. These domains happen equally at all length scales, so the cut-off scale ξ_x vanishes. These fronts follow intrinsic anomalous scaling, as seen in Fig. 2.6(c) by the structure factor being time-dependent. Exponents observed depend continuously on disorder strenght, however, so no universality is present.

In the one-sided model, nucleation of domains of the advancing phase is kinetically suppressed by $M = 0$ in the receding phase. Due to this the cut-off ξ_x remains, as seen in the structure factors in Fig. 2.6(f). The resulting non-universal scaling picture of the one-sided model at strong disorder agrees with Hele-Shaw experiments at strong disorder [11]. This is valid for growth exponents as well roughness. Thus we conclude that the one-sided phase field model is valid for the description of the Hele-Shaw experiment at strong disorder, and that universal scaling isn't found in either as exponents depend continuously on the disorder strength.

3. Diffuse Interface Thermohydrodynamics Models

The Model B phase field model considered in the context of the Hele-Shaw cell and kinetic roughening of interfaces above is valid for flows that are slow and viscosity dominated. A natural extension is to take advective properties into account. Direct extension of the Model B would be a Cahn-Hilliard - Navier-Stokes system considered for example in Refs. [41, 42]. In that model, the free energy is exactly the same Cahn-Hilliard form (2.11) as in the phase-field Model B above. The Cahn-Hillard free energy is coupled with Navier-Stokes incompressible hydrodynamics by incorporating a force from the chemical potential gradient into the momentum equation, and the phase field dynamical (continuity) equation is a hybrid diffusion-advection equation. This kind of model, like the Model B, describes a two-component system of phases that don't change into one another, such as air and water.

In our work we were more motivated by modeling boiling, which calls for single-component liquid/vapor flow, where the two phases can change into one another and are characterized by different densities. Also in liquid-vapor flows thermal effects are central due to latent heat. As described in the introduction, the first liquid-vapor model was introduced by Van der Waals[1], and to this day the Van der Waals (VdW) model is a central benchmark case in modeling liquid-vapor flows [27, 28, 31].

The original Van der Waals theory describes the thermodynamics of a prototype liquid/vapor system in equilibrium, where by definition no flows are taking place. To make the theory describe advective dynamics, one needs to describe the forces that act when the system is off equilibrium. Furthermore we need the interface tension of the liquid/vapor interface. These are obtained in the Van der Waals theory by assuming that the equation of state is valid point-wise, giving the pressure as function of density and temperature even off-equilibrium. A square-gradient energy

cost gives the interface tension as density changes between gas and liquid in analogue to the phase-field theory.

For the dynamic theory to be valid we must assume that molecular time scales relaxing to a local equilibrium are much slower than the dynamics of the fields of the system. Then the equation of state is meaningful off-equilibrium. It is worthwhile to note that it is not necessary for the equation of state to be strictly valid in the interfacial region where the density changes through the unstable regime between the two densities. As long as the interface width is smaller than other physical scales the description of the interface with a diffuse interface, with "bulk" and gradient energy contributions, is equivalent to setting the surface tension in the model.

The equilibrium VdW theory is described by the Helmholtz free energy per volume [1]

$$f(\rho,T) = k_B T \frac{\rho}{m_p}\left(\log\left(\frac{\frac{\rho}{m_p}(k_B T)^{-3/2}}{1-b\frac{\rho}{m_p}}\right)-1\right) - a\left(\frac{\rho}{m_p}\right)^2, \tag{3.1}$$

and the corresponding VdW equation of state is obtained as

$$p(\rho,T) = \rho\partial_\rho f(\rho,T) - f(\rho,T) = \frac{k_B T\frac{\rho}{m_p}}{1-b\frac{\rho}{m_p}} - a\left(\frac{\rho}{m_p}\right)^2. \tag{3.2}$$

The internal energy can also be straightforwardly calculated from thermodynamics

$$e(\rho,T) = f(\rho,T) - T\partial_T f(\rho,T) = \frac{3k_B}{2m}T\rho - \frac{a}{m^2}\rho^2. \tag{3.3}$$

In the above we have the pressure, density, temperature, Boltzmann constant and molecular mass as p, ρ, T, k_B and m_p, respectively. The VdW parameters a and b describe the fluid in question. Several relatively simple extensions to the VdW equation of state have been presented for various engineering purposes, and the dynamic theory here presented should be equally valid for them as well[43]. Here we focus on the VdW fluid as the benchmark and prototype.

The interface tension is added to the model by assuming that the free energy and equation of state are valid point-wise, and that gradients of density have an associated energy cost, as density is the order parameter separating the gas and liquid. The Helmholtz free energy is then given by

$$F = \int \mathrm{d}x \left[f(\rho(x),T(x)) + \frac{\kappa}{2}|\nabla\rho(x)|^2 \right]. \tag{3.4}$$

The gradient energy coefficient κ determines both the surface tension and the width of the interface in the model. The surface tension is[14]

$$\sigma = \sqrt{2\kappa}\int_{\rho_g}^{\rho_l} \mathrm{d}\rho\sqrt{\Delta f(\rho,T)}, \tag{3.5}$$

where ρ_g and ρ_l are the gas and liquid densities at coexistence at temperature T. $\Delta f(\rho)$ is the difference between value of $f(\rho)$ and the double tangent line at ρ. The gradient energy coefficient can be made to depend on density and temperature, as considered by several authors [29, 44, 28]. Here, for simplicity, we assume a constant gradient energy coefficent $\kappa = \text{const}$. With this assumption the interface tension can be matched experimentally at one temperature, and a qualitatively reasonable behavior for it is predicted by the VdW theory as a function of temperature and pressure. For example, the interface tension vanishes continuously when going to the critical point.

Above the Helmholtz free energy describes energetics of a VdW system, which is generally off equilibrium. Connection from the energetics to hydrodynamics is given by the pressure, which in a diffuse interface description is a tensor containing gradients of density, and possibly temperature. The connection, originally by Korteweg[26], is based on the equilibrium pressure tensor the equilibrium free energy being consistent. At equilibrium the pressure tensor has zero divergence, whereas the Helmholtz free energy is at minimum, i.e. zero functional variation w.r.t. density

$$\nabla \cdot P = 0 \quad \Leftrightarrow \quad \frac{\delta F}{\delta \rho}. \tag{3.6}$$

This is achieved with the pressure tensor

$$P_{ij}^T = \left(p(\rho, T) - \kappa\rho\partial_k{}^2\rho - \frac{1}{2}\kappa\partial_k\rho\partial_k\rho \right)\delta_{ij} + \kappa\partial_i\rho\partial_j\rho. \tag{3.7}$$

We use the Einstein summation notation, and the shorthands $\partial_i = \partial_{x_i}$, for all indices i, j and k. The superscript ^{T} signifies that the Korteweg tensor above assumes constant temperature. Note also that the argument presented in Eq. (3.6) contains differentiations on both sides. That means that the above diffuse interface pressure tensor and the free energy are consistent with each other, but they are not uniquely defined by the derivation.

The standard compressible hydrodynamic equations for a fluid motion with the stress tensor above read

$$\partial_t\rho + \partial_j(\rho v_j) = 0\,; \tag{3.8}$$

$$\partial_t(\rho v_i) + \partial_j(\rho v_i v_j) = -\partial_j P_{ij}^T + \partial_j\sigma_{ij} + g_i, \tag{3.9}$$

where v_i is the velocity field, σ is the viscous stress and g contains external bulk forces, such as gravity. Thus we have arrived at a description of the liquid/vapor flow that is very different and significantly more complicated

than the phase field Model B equation (2.9). The flow of the density, which is now the order parameter, is completely determined by the advective velocity v, in particular there is no diffusive mass flux.

The question for the diffuse interface pressure tensor becomes more complicated when the case is not isothermal. In a gas-liquid phase transition the thermal effects are expected to be especially important and large temperature differences present near the interface due to latent heat released or absorbed. The basis of coupling the thermal field to the pressure tensor above is that the capillary forces due to the gradient energy act adiabatically. Based on this, two extensions to the isothermal pressure tensor above has been obtained. Anderson considered an additional heat flux in addition to Fourier's law, proportional to density and temperature gradients and κ [27, 44]. Onuki derived a formulation where the pressure tensor itself was extended [28]. Recently, both the Anderson [31] and the Onuki [30] approaches have been succesfully used to study various numerical examples.

A gas-liquid model will also need to account for the different thermal conductivities and viscosities in the liquid than in the gas. For our purposes we used a simple constant times density for both. Using these, the model for full VdW thermohydrodynamics of Anderson *et al.* [27] becomes

$$\partial_t \rho + \partial_j(\rho v_j) = 0 \; ; \tag{3.10}$$

$$\partial_t v_i + \partial_j(\rho v_i v_j) = -\partial_j P_{ij} + \eta_0 \partial_j \left[\rho \left(\partial_i v_j + \partial_j v_i\right)\right] + \rho g_i \; ; \tag{3.11}$$

$$\begin{aligned} \partial_t e(\rho,T) + \partial_j(e(\rho,T)v_j) &= -P_{jk}\partial_j v_k + \eta_0 \left[\rho \left(\partial_j v_k + \partial_k v_j\right)\right] \partial_j v_k + \\ &\quad + \alpha_0 \partial_j \left(\rho \partial_j T\right) - \kappa \partial_j \left(\rho \left[\partial_k v_k\right] \partial_j \rho\right) \; ; \end{aligned} \tag{3.12}$$

$$\begin{aligned} P_{ij} &= \left(p(\rho,T) - \kappa\rho{\partial_k}^2\rho - \frac{1}{2}\kappa\partial_k\rho\partial_k\rho\right)\delta_{ij} + \\ &\quad + \kappa\partial_i\rho\partial_j\rho. \end{aligned} \tag{3.13}$$

The model by Onuki *et al.* [28] becomes

$$\partial_t \rho + \partial_j(\rho v_j) = 0 \; ; \tag{3.14}$$

$$\partial_t v_i + \partial_j(\rho v_i v_j) = -\partial_j P_{ij} + \eta_0 \partial_j \left[\rho \left(\partial_i v_j + \partial_j v_i\right)\right] + \rho g_i \; ; \tag{3.15}$$

$$\begin{aligned} \partial_t e(\rho,T) + \partial_j(e(\rho,T)v_j) &= -P_{jk}\partial_j v_k + \eta_0 \left[\rho \left(\partial_j v_k + \partial_k v_j\right)\right] \partial_j v_k + \\ &\quad + \alpha_0 \partial_j \left(\rho \partial_j T\right) \; ; \end{aligned} \tag{3.16}$$

$$\begin{aligned} P_{ij} &= \left(p(\rho,T) - \kappa\rho{\partial_k}^2\rho - \frac{1}{2}\kappa\partial_k\rho\partial_k\rho + \frac{\rho}{T}\partial_k\rho\partial_k T\right)\delta_{ij} + \\ &\quad + \kappa\partial_i\rho\partial_j\rho. \end{aligned} \tag{3.17}$$

Here e is the internal energy, which is total energy minus kinetic energy. Note the differences in the additional term in the energy equation (3.12)

in Anderson's formulation, and the pressure tensor (3.17) in Onuki's formulation.

In our work on boiling, we used Onuki's model, to which we developed boundary conditions so that the physics of boiling on a heated surface under constant external pressure is obtained.

3.0.1 Boundary Conditions

To capture relevant physics with the gas-liquid model we need to incorporate appropriate boundary conditions. Although laboratory experiments on controlled boiling has been performed with spot heating by lasers [45], practical boiling happens at a hot wall and under constant external pressure. This means boundary conditions are needed in the computational system need to account for the hot wall, and the wetting properties of this wall are relevant. To set constant external pressure we need to set an open boundary condition that is artificial in the sense that the location of the boundary purely a numerical necessity and the physics must not depend on the location of this imaginary boundary. Outside this imaginary boundary of our computational domain, we have an infinite bulk to which we ascribe temperature and pressure according to the external environment of our boiling system of interest. As long as the open boundary as far enough from the interesting dynamics of the system, the dynamics and physics do not depend on the location of the boundary. Physics will crucially depend on the temperature and pressure we set at the open boundary, though, as it should since this is the physical environment where the boiling happens.

Physical walls for the VdW fluid have earlier been considered as completely wet by a precursor liquid film [28, 30]. If the liquid-gas interface never comes into contact with the wall, the wetting properties of the wall become irrelevant [32]. Concurrently with our work, a wall with controlled wetting properties has also been introduced by Teshigawara *et al.*[46]. An open boundary condition along the lines we describe in Publication IV with an external pressure prescribed, is a novel development. Keeping the pressure of the system at coexistence while boiling was earlier considered by allowing a (large) gas pocket far away from the boiling surface[28]. This leads to an approximation of boiling in an open system by observing only the immediate vicinity of the hot wall. The quality of the approximation is uncertain, and experimentally the small scales in

these simulations cannot be probed for verification.

Wettability of a solid wall comes from different surface energies if the wall is in contact with gas or liquid, σ_{sg} and σ_{sl}, respectively. Together with the liquid-gas (σ) interface tension, these give the equilibrium contact angle Θ_e described by Young's equation

$$\cos(\Theta_e) = \frac{\sigma_{sg} - \sigma_{sl}}{\sigma}. \tag{3.18}$$

From Young's equation, the methodology of Jacqmin *et al.*[41] allows obtaining an exact boundary condition for the order parameter in the case of the Cahn-Hilliard free energy. For the VdW free energy the equivalent condition is approximate, but in Publication IV we verify that this approximation is valid within a few degrees. Using Jacqmin's approach our boundary condition for a constant temperature (T_{wall}) wall with and σ_{sg} and σ_{sl} becomes

$$\begin{aligned}
v_i &= 0 \quad \text{, for every i ;} && (3.19)\\
\nabla_n \rho &= \frac{\sigma \cos\Theta_e}{\kappa} \partial_\rho g_T(\rho) && (3.20)\\
T &= T_{wall}; && (3.21)\\
\nabla_n P_{ij} &= 0 \,, && (3.22)
\end{aligned}$$

where ∇_n is the gradient in the direction normal to the wall. We consider a wall which is heated to constant temperature. A more complicated boundary condition would be needed for a wall that has constant heat flux, or otherwise variable temperature.

We obtain the open boundary condition that sets a bulk with prescribed temperature and pressure by setting temperature, density and pressure. To practically make this in our numerics, we also introduce pressure as an additional variable in the equations to solve. Since the equation of state ties together the temperature, density and pressure, the values must be set so that the equation of state is fulfilled. In other words the density must be either the gas or the liquid density at the temperature and pressure prescribed. Note that unless the temperature and pressure are exactly at the boiling point, one phase will be stable and the other metastable. The open boundary condition of a fixed pressure reads

$$\begin{aligned}
\nabla_n v_i &= 0 \quad \text{, for every i ;} && (3.23)\\
\rho &= \rho_{wall}, && (3.24)\\
T &= T_{wall}, && (3.25)\\
P_{ij} &= p_{wall}\delta_{ij}, && (3.26)
\end{aligned}$$

where for physical consistency it must hold that $p(\rho_{wall}, T_{wall}) = p_{wall}$.

It is worthwhile to note that an open boundary set with the homogenous Neumann boundary for velocity like above will be fully reflecting in terms of sound (compressibility) waves. Advanced boundary conditions to prevent unphysical reflections from the artificial boundary have been studied and developed for one-phase hydrodynamics [47]. However, in our work we assume that the sounds waves will not affect the dynamics of phase change. The phase change obviously does emit sound but we consider the reverse to be irrelevant in the cases we study. Thus we do not attempt to fully resolve the compressibility waves. The basis of this is that the density differences in sounds waves is of the order of one percent to that of the density difference between the phases.

3.0.2 Dimensionless Units and Physical Scales

A feature of the diffuse interface method is that given the gradient energy coefficient and the (bulk) free energy, the interface tension and the width of the equilibrium gas-liquid interface is determined. In other words given the bulk properties of the fluid, in our case the VdW fluid and the interface tension, the width of the interface is predicted by the square gradient diffuse interface method. The width of the interface is the smallest physical scale that must be resolved by the model, and as such it sets the scale at which simulations can be performed.

For numerical purposes we need to transform the model to dimensionless units. This is also convenient in that a number of parameters equal to the number of physical scales can be removed when considering the system in units given by the parameters. In the Model B phase field model we scaled out the mobility by the time scale, and the gradient energy coefficient or equivalently the interface width by the length scale. In the VdW system, we observe the system in such units that the critical point (T_c, p_c, ρ_c) in dimensionless temperature, pressure and density equals unity.

Observing the VdW system in units where the critical point is at unity means the physical scales that correspond to the dimensionless ones depend on material parameters of the physical fluid we model. The VdW fluid isn't a quantitative model for real fluids but we match it to properties water at $T = 0.5T_c$, and thus obtain a qualitatively reasonable model. That means that all material properties of the fluid, including inteface

tension, thermal conductivity and viscosity are of the correct order of magnitude over the temperature and density range we consider.

The unit scales where the critical point of the VdW fluid is at unity are given, as function of the material parameters, by

$$x_0 = 2b^{1/3}\,; \tag{3.27}$$

$$m_0 = \frac{8}{3}m_p\,; \tag{3.28}$$

$$t_0 = 6b^{5/6}\sqrt{\frac{m_p}{a}}. \tag{3.29}$$

With the critical properties of water: $T_c = 647$ K, $p_c = 22.1$ MPa, $\rho_c = 322$ kg/m^3, we obtain the characteristic length $x_0 = 0.74$ nm, time $t_0 = 2.8$ ps, and mass $m_0 = 1.3 \cdot 10^{-25}$ kg. The thermal conductivity and viscosity scale trivially with their physical units. The connection between the dimensionless gradient energy coefficient $\tilde{\kappa}$ and the physical interface tension is more complex, coming from Eq.(3.5)

$$\tilde{\kappa} = \frac{t_0^4\sigma^2}{2m_0^2\left[\int_{\tilde{\rho}_g}^{\tilde{\rho}_l} \mathrm{d}\tilde{\rho}\sqrt{\Delta\tilde{f}(\tilde{\rho})}\right]}. \tag{3.30}$$

Choosing the dimensionless coefficients

$$\tilde{\eta}_0 = 1 \tag{3.31}$$

$$\tilde{\alpha}_0 = 30 \tag{3.32}$$

$$\tilde{\kappa} = 1, \tag{3.33}$$

leads to the following dimensional properties for our VdW fluid at $0.5T_c$: kinematic viscosity $\eta_0 = 2 \cdot 10^{-7}\frac{\mathrm{m}^2}{\mathrm{s}}$, heat conductivity per density $\alpha_0 = 6 \cdot 10^{-4}\frac{\mathrm{J\ m}^2}{\mathrm{kg\ K\ s}}$, and interface tension $\sigma = 0.07\frac{\mathrm{N}}{\mathrm{m}}$. The lambda value for the liquid is then $\lambda_l = 0.7\frac{\mathrm{W}}{\mathrm{K\ m}}$.

3.1 Numerical Integration of Diffuse Interface Thermohydrodynamics

The diffusive dynamics of the Model B phase field model is easily solved numerically by the explicit or implicit Euler methods. Much more care needs to be put for the numerical methods in hydrodynamics, that is when advective velocities are dominant. Computational methods for the Navier-Stokes equations of incompressible single-phase flow have been developed for several decades[48]. In our boiling model the case is complicated by

the fact that the flow is compressible, and that we need adaptive grid refinement to resolve out the interface efficiently. Adaptive grids are readily available in the finite element method (FEM). The characteristics-based-splitting (CBS) time integration algorithm for time-dependent compressible flows, particularly with FEM in mind, has recently been developed by Zienkiewicz *et al.*[36, 35], and this is the basis of our method to integrate two-phase thermohydrodynamics.

The standard CBS method solves for the time evolution of density and momentum and assumes a temperature equation that can be set in addition like a passive scalar [36]. This is insufficient for the gas-liquid phase change, however. When the phase changes between gas and liquid at the interface, the latent heat means that the temperature equation is affected as strongly as the density. This means that for the two-phase thermohydrodynamics we must extend the CBS method to consider the temperature equation just like it does the continuity equation, not like a passive scalar. In other words, the temperature is included in the pressure correction step. The details of the numerical method are presented in Publication IV of this thesis.

3.2 Isothermal Verification of the Boiling Model

We carefully verify each part of our boiling model using isothermal simulations. The numerical cases studied and compared against theoretical predictions are presented in Figure 3.1. Laplace pressure, the pressure increase inside a bubble due to interface tension, offers a sensitive way to check the validity of our numerical scheme. Laplace pressure increase for a 2D bubble of radius r is

$$\Delta p = \frac{\sigma}{r}. \tag{3.34}$$

When the avearge density is in the coexistence region, a stable bubble is the equilibrium solution of the gas-liquid model in a closed system where the boundaries are physical walls. The pressure values inside and outside the bubble are obtained directly from the density via the equation of state. Figure 3.2 shows the surface tension values obtained. The model actually reproduces the density changes due to the Laplace pressure difference to about the fourth decimal. This is somewhat surprising because the density values match their theoretical coexistence values only to the second decimal.

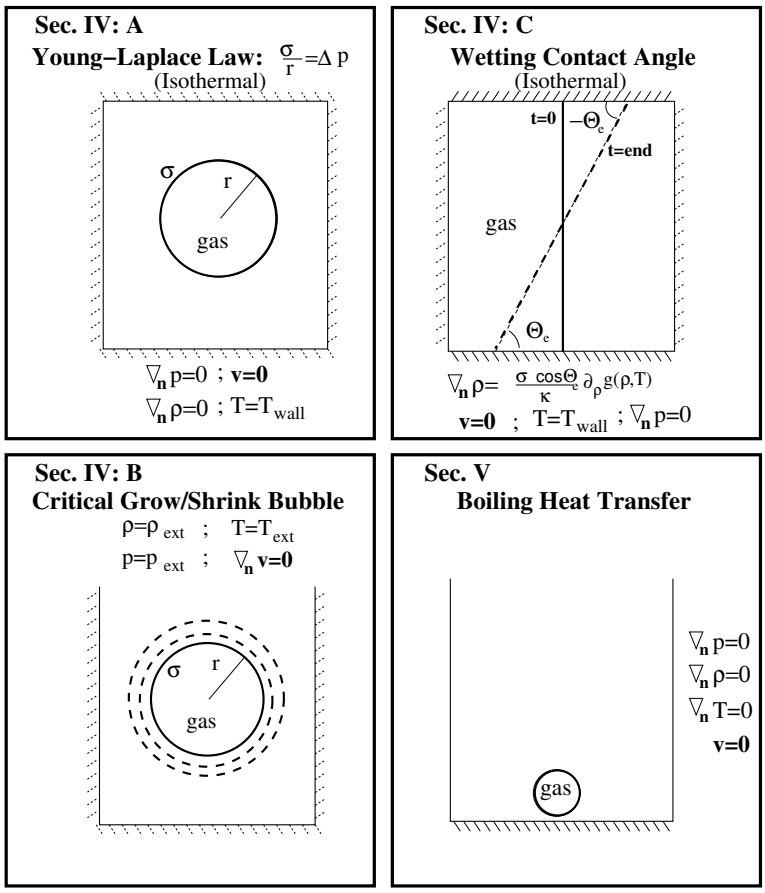

Figure 3.1. A schematic view of the simulations with their corresponding boundary conditions is illustrated here. We simulate the Young-Laplace law for a single bubble immersed in its coexistence liquid. We verify the open boundary condition by comparing with an analytical solution. The proposed wetting boundary condition is verified in simulations of isothermal systems but for different temperatures. Numerical simulations of boiling in a domain with a temperature gradient, where the upper boundary allows an in- and out-flux of mass.

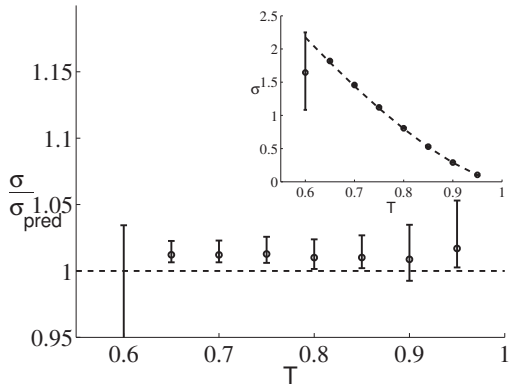

Figure 3.2. Interface tension of a bubble in an isothermal system. Interface tension data as obtained from observed pressure difference between the gas and liquid domains. The inset shows raw data, which is scaled with the predicted values from Eq. (3.5). At temperatures above $T = 0.65$, we observe interface tensions within 5% of the predicted ones.

We verify the open boundary condition, the main novel feature in our model, via homogenous nucleation theory. By imposing the external pressure and temperature so that the gas phase is stable and the liquid phase is metastable, homogenous nucleation theory states that a bubble will grow or shrink depending on which way locally decreases Gibb's free energy of the system. There will be a limiting size to the bubbles in the system, smaller than which will shrink and larger will grow. We calculate a prediction for this limiting size, shown in detail in the Appendix of Publication IV, and compare the results with numerical ones in Figure 3.3. The numerical limiting bubble size is obtained by starting with different bubble sizes as initial condition, and letting it run until obvious growth or shrinkage is observed. Since the limiting radius is a unstable equilibrium the closer we get the slower the dynamics will be. Eventually numerical effects and sounds waves make it too CPU intensive to conclusively say whether the initial bubble will grow or collapse.

We note the theoretical estimate for the limiting bubble size is an approximation, and the initial condition of the bubble cannot be set to exactly match quasi-static conditions. Both of these araise from the fact that pressure is not constant in the gas-liquid system - only the external pressure is set. Regardless, the agreement found between the numerical results and the theoretical estimate is satisfactory, and shows that our open constant pressure boundary works in a physically correct way.

Finally we verify the boundary condition of the physical wall whose wet-

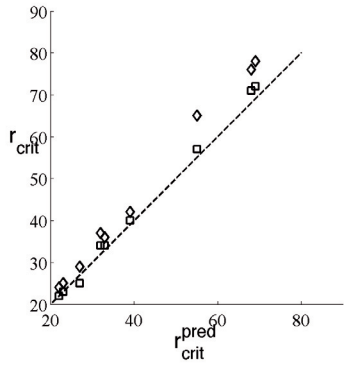

Figure 3.3. Numerically observed limiting radius of a bubble that will grow in superheated liquid, plotted against prediction obtained from homogenous nucleation theory. Stars are lower bound observations, diamonds upper bound. Solid line is our analytical estimate.

ting parameters we want to impose. Since we wish to impose the contact angle, we set a system with a planar gas-liquid interface across it, and set the interface to meet opposing wall at contact angles of opposite sign. The equilibrium solution is then a straight, planar interface at the set angle, and we can measure this angle comparing it to the value we theoretically set with our boundary condition. The errors we measure between the theoretical and observed values are shown in Figure 3.4. The numerical contact angle is a few degrees towards the perpendicular compared to what it should be imposed to. We conclude that the contact angle is reproduced to sufficient accuracy, especially as compared to how well the contact angles are experimentally known for various surfaces [49].

3.3 Numerical Simulation of Boiling at Constant Pressure

With the thermohydrodynamic model verified, we can finally study the microscale dynamics of boiling at constant pressure and control the wetting properties of the boiling surface. Imaging in this regime is extremely difficult in experiments [25, 22, 49]. According to the vapor recoil theory it is the growth of a single bubble in the microscopic regime, whether the bubble will grow spherically or spread along the heating surface, that determines the transition between nucleate boiling and film boiling.[23, 25].

InPublication IV we show that both nucleate and film boiling regime are obtained in our model when different surface wetting properties are used.

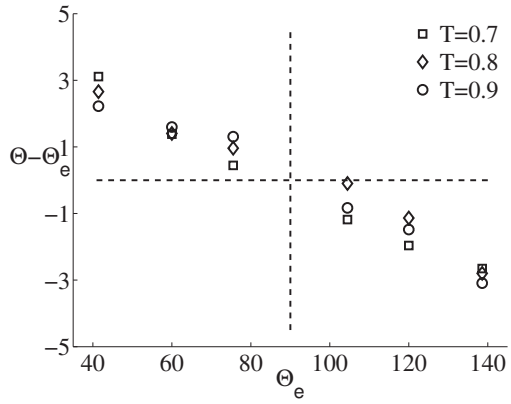

Figure 3.4. Contact angle measured in a system with a straight interface across it. The difference between measured contact angle at numerical equilibrium and the imposed one, as a function of the set contact angle, in degrees. Six different Θ values were measured in three temperatures each.

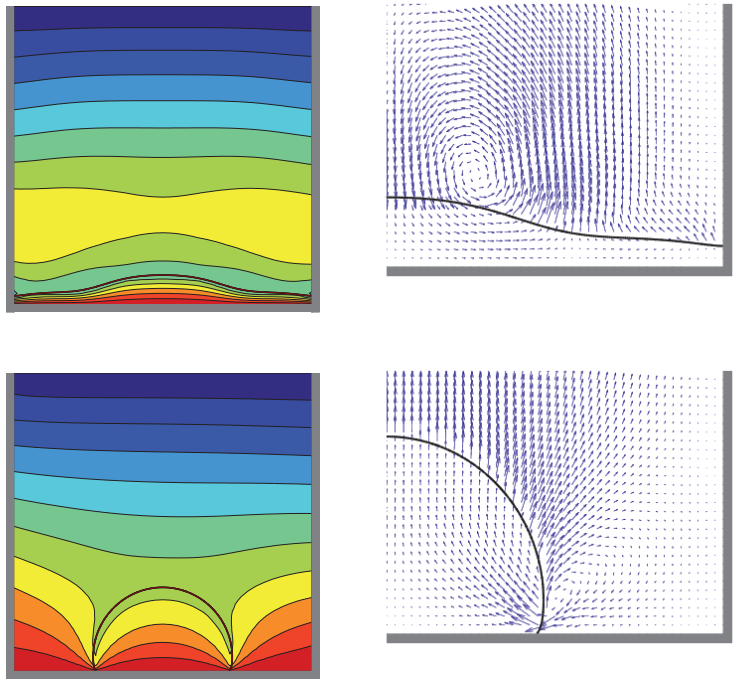

Figure 3.5. The temperature field and the mass flux vector field of boiling with the hot lower wall having different surface wettability. The black line is the gas-liquid interface, or density contour at the average of gas and liquid. A hydrophobic wall leads to film boiling, whereas nucleate (bubble) boiling persists on a hydrophilic wall.

We observe boiling with the lower wall being the hot boiling surface at $T = 0.9T_c$. At the top boundary of the system we set $T = 0.88T_c$, and the constant pressure is set so that the boiling temperature is $T_b = 0.89T_c$. Figure 3.5 shows the boiling cases obtained when a nucleate bubble is seeded near the hot wall and let to evolve towards a steady boiling regime. The upper images show the case of a strongly hydrophobic boiling surface, ($\Theta_e = 177°$), and the lower images show the case of a hydrophilic surface ($\Theta_e = 45°$). Apart from boiling surface wettability all parameters are the same. The black line is the gas-liquid interface obtained from the density field, which rapidly changes between liquid and gas at the interface, being otherwise uninteresting.

In the case of a hydrophobic wall we obtain film boiling. The gas film that is rapidly generated at the wall acts to insulate the hot wall from the liquid, which drastically reduces the boiling rate. If the wall is hydrophilic nucleate boiling is observed, where the bubble retains a spherical shape as it grows. A thermodynamic driving force by the temperature gradient drives the bubble towards the hot wall, and the gas-liquid interface touches the hot wall as the semi-spherical bubble grows. The interface, and by extension also the contact line "foot" of the bubble is on the other hand being maintained at the boiling point temperature due to boiling and latent heat. This leads to a very high influx of heat into the system at the contact line, and thus a very high boiling rate in a small area around the contact line. The spherical bubble will continue to grow at a constant rate, since the contact line foot of the bubble will be unchanged, only moving along the boiling surface as the bubble grows.

At the foot of the nucleate boiling bubble we observe a vortex of mass flux, seen in lower right image of Fig.3.5, and the mass flux at the contact line is seen to be into the bubble. We interpret this as verification from the full microscale thermal hydrodynamics that the mechanism assumed by the vapor recoil theory exists and the forces it imples distort the interface profile at the contact line [50, 23]. Boiling at constant pressure, that is the latent heat keeping the interface temperature close to the boiling point at the pressure, is found to be crucial in creating the vapor recoil effect. To our knowledge our work is the first time a numerical method of full microscale thermohydrodynamics that can be considered predictive for boiling at constant pressure is achieved, and with this method we detect the vapor recoil mechanism.

The two dimensional case we considered can give relevant insight into

the physics of boiling, but to account for the third dimension are a necessary extension to our methodology if the vapor recoil or other features of bubble growth during boiling, are to be qualitatively predicted. Cylindrical coordinates are the computationally lest demanding way to take the third dimension into account [30]. This is crucial because the circumference of the contact line at the foot of the bubble grows as the bubble grows. In our two-dimensional simulations the foot of the bubble just simply moves. The extending contact line is important because the amount of boiling, the heat transfered from the hot surface to the fluid, is strongly dependent on the length of the contact line. The balance between the surface tension keeping the growing bubble spherical and the vapor recoil pushing the bubble to spread flat along the boiling surface is the key to how the vapor recoil explains the critical heat flux. It is unclear how much of these dynamics is captured by the two-dimensional picture, but to predictively determine it one would need the full three-dimensional case, since as mentioned, there are no experimental observations of the flow fields to compare to.

Another relevant and interesting extension to our model would be to consider the boiling surface to have a constant heat flux as opposed to constant temperature. Preferably heat transfer along the hot wall, towards the contact line spots where boiling happens, would also be included. This demands a non-trivial modification to our wetting boundary condition to model surface energies at the wall, however.

4. Summary

In this thesis we have considered numerical modeling of two-phase fluid flows. The approach we employ sets an energy cost for gradients of the order parameter, and so creates surface tension in the model. The approach was first considered in the 19th century by Van der Waals, and is in modern parlace known as the phase field, or equivalently diffuse interface methodology.

First we considered slow flows, as happens by groundwater and fluids otherwise penetrating granular media. Experimentally these kind of flows have been studied via the Hele-Shaw cell setup. Our model of choice for these flows is a Model B -type phase field method, which describes flows where viscosity dominates. We develop phase field type models that describe Hele-Shaw experiments. We model the Hele-Shaw cell at coarse scale as a two-dimensional system with randomness to account for variations in the gap in the Hele-Shaw, and thus capillary pressure.

We match our phase field model to two types of Hele-Shaw experiments, where the fluid flow is driven either spontaneously or via a constant volume flux. The phase field model is simple enough that a analytic projection scheme can be performed to analyze the roughening of the wet-dry interface. We also considered a more microscopic phase-field model for the Hele-Shaw cell, where the model is three-dimensional, and fluctuations are present explicitly in the location of the wall of the cell. A Green's function based method to make it possible to analyze the fluctuating wall in terms of the projection method is developed.

Finally with the phase-field model we find the extent of validity of the projection method, which is based on a perturbative expansion in small fluctuations of the wet-dry interface, by increasing the strenght of the disorder. Our conclusions with the phase field models are that the results of the Hele-Shaw experiments in the various cases and parameters con-

sidered can be consistently reproduced by the phase-field models. In more general terms as a universality class of kinetic roughening when the order parameter is conserved, we find the scaling properties of the phase field model and the Hele-Shaw cell to vary quite significantly among the (still limited) different cases we considered. Since these are both minimal model systems to account for the potential universality class, we have to conclude that our studies suggest that universality in systems dominated by conservation laws will be sparse and hard to find.

We also consider two-phase flows dominated by advection. Pure fluid liquid-gas flows, commonly known as boiling and condensation, are technologically important and scientifically challenging. Boiling is a very attractive method for heat transport and the maximum heat transport by boiling is limited by the boiling crisis. We develop numerical methodology to study liquid-gas flow at microscopic length and short time scales. This is in stark contrast to the scales of the Hele-Shaw cell and the Model B phase field. The compressible fluid dynamics, extended to account for the interfaces that the liquid-gas flows entail, are considerably more difficult to solve numerically than Model B. To apply the numerical methdos involved, we applied a toolbox created by our collaberators called femLego. This makes solution of any field equations much simpler for the physisict, and crucial for our applications adaptive meshes are readily included.

The liquid-gas flow methodology developed in this thesis allows to numerically study boiling under constant pressure, which is a crucial condition to study practical boiling. We make a tentative study of bubbles seeded near a hot boiling surface with different wetting conditions. The study shows that we can obtain both film boiling and nucleate boiling. For nucleate boiling we show the full thermohydrodynamic profile near the contact line of the bubble, and in particular we observe a vortex which ejects mass into the bubble which is growing at the expense of the liquid. We interpret this as verification of the vapor recoil mechanism and the first observation of its microscopic properties. The vapor recoil is though to be crucial in the boiling crisis, which is transition between nucleate boiling as bubble and film boiling.

The goal of the microscopic liquid-gas flow model is to be predictive enough to conduct numerical experiments of boiling at the microscale, particularly studying the transition between nucleate boiling and film boiling under different parameters of the heat flux, surface wettability and temperature. This is relevant particularly because experimental ob-

servations in this scale are extremely hard to do. In the near term modeling such as we performed here is limited to the microscopic length and time scales. But this is precisely the scales where simulations can offer information complimentary to experiments once model development reaches a stage that numerical experiments are trusted to be predictive. Several immediate extensions of the model would be interesting in terms of future work. Writing the model for cylindrical coordinates to account for the third dimension is one such extension. Another would be to give the boiling surface a finite heat conductivity and let it be heated by a controlled heat flux as opposed to temperature. The modeling approach we've developed here, both in terms of the the theory and the numerical solution methods, would hopefully answer plenty of interesting questions in boiling and boiling crisis, enabling to study the behavior of growing bubbles as a function of all the relevant physical parameters.

Bibliography

[1] J.D. Van der Waals, Verh.-K. Ned. Akad. Wet., Afd. Natuurkd., Eerste Reeks **1**, 56 (1893) ; J.S. Rowlinson, J. Stat. Phys. **20**, 197 (1979)

[2] White, F. M. *Viscous Fluid Flow* 3rd ed. (McGraw-Hill, Boston, 2005)

[3] *http://www.claymath.org/millennium/Navier-Stokes_Equations*

[4] C. T. Crowe (ed.) *Multiphase Flow Handbook*, (CRC Press, 2006)

[5] M. Dube, M. Alava, M. Rost, Advances in Physics **113**, 83 (2004)

[6] T. Halpin-Healy and Y.-C. Zhang, Physics Reports **254**, 215 (1994)

[7] A.-L. Barabasi, H. E. Stanley, *Fractal Concepts in Surface Growth* (Cambridge University Press, Cambridge, 1995).

[8] Joachim Krug, Advances in Physics **46**, 139 (1997)

[9] L. P. Yarin *et al.*, *Fluid Flow, Heat Transfer and Boiling in Micro-Channels* (Springer-Verlag, Berlin, 2009)

[10] J. Soriano, J. Ortín and A. Hernández-Machado, *Phys. Rev. E*, **66** 031603 (2002)

[11] J. Soriano, J. Ortin, A. Hernández-Machado, Phys. Rev. E **67**, 056308 (2003)

[12] E. Pauné and J. Casademunt, Phys. Rev. Lett. **90**, 144504 (2003)

[13] D. Geromichalos, F. Mugele and S. Herminghaus, Phys. Rev. Lett. **89**, 104503 (2002).

[14] J.W. Cahn, J.E. Hilliard, J. Chem. Phys. **28**, 258 (1958)

[15] M. Dubé, M. Rost, K. R. Elder, M. Alava, S. Majaniemi, T. Ala-Nissila, Phys. Rev. Lett. **83**, 1628 (1999); Eur. Phys. J. B **15**, 701 (2000); Phys. Rev. E **64**, 051605 (2001)

[16] P. C. Hohenberg and B. I. Halperin, Rev. Mod. Phys. **49**, 435 (1977)

[17] K. R. Elder, M. Grant, N. Provatas, J.M. Kosterlitz, Phys. Rev. E **64**, 021604 (2001)

[18] T. Laurila, C. Tong, I. Huopaniemi, S. Majaniemi and T. Ala-Nissila, Europ. Phys. Journal B **46**, 553 (2005)

[19] T. Laurila, C. Tong, S. Majaniemi, T. Ala-Nissila, Physical Review E **74**, 041601 (2006)

[20] T. Laurila, M. Pradas, A. Hernandez-Machado, T. Ala-Nissila, Physical Review E **78**, 031603 (2008)

[21] V. K. Dhir, Annu. Rev. Fluid Mech. **30**, 365 (1998)

[22] T. G. Theofanous *et al.*, Exp. Therm. Fluid Sci. **26** 775-810 (2002)

[23] V. S. Nikolayev and D. A. Beysens, Europhys. Letters **47**, 345 (1999)

[24] V.S. Nikolayev *et al.*, Microgravity Sci. Technol. **18**, 34 (2005)

[25] V. S. Nikolayev *et al.*, Phys. Rev. Lett. **97**, 184503 (2006)

[26] D. Korteweg, Arch. Neerl. Sci. Exactes Nat. Ser II **6**, 1 (1901)

[27] D.M. Anderson, G.B. McFadden, A.A. Wheeler, Annu. Rev. Fluid Mech. **30**, 139 (1998)

[28] Akira Onuki, Phys. Rev. E **75**, 036304 (2007)

[29] J.E. Dunn and J. Serrin, Arch. Rat. Mech. Anal. **88**, 95 (1985)

[30] R. Teshigawara and A. Onuki Phys. Rev. E **82**, 021603 (2010)

[31] A. Pecenko, J.G.M. Kuerten, C.W.M. van der Geld, Int. J. Multiphase Flow **36** 558 (2010)

[32] A. Pecenko, L.G.M. van Deurzen, J.G.M. Kuerten, C.W.M. van der Geld, Int. J. Multiphase Flow **37** 149 (2010)

[33] M. Do-Quang, W. Villanueva, I. Singer-Loginova, and G. Amberg, Bull. Pol. Acad. Sci-Te **55**, 229 (2007)

[34] G. Amberg, R. Tonhardt, C. Winkler, Math. and Comput. Simulat. **49**, 149 (1999)

[35] P. Nithiarasu, R. Codina, O.C. Zienkiewicz, Int. J. Numer. Meth. Engng **66** 1514

[36] O. C. Zienkiewicz, R. L. Talyor and P. Nithiarasu, *The Finite Element Method for Fluid Dynamics* 6th ed. Elsevier (2005).

[37] J. M. López and M. A. Rodríguez, Phys. Rev. E **54**, R2189 (1996)

[38] M. Dubé, M. Rost, M. Alava, Eur. Phys. J. B **15** 691, (2000)

[39] J. J. Ramasco, J. M. López, M. A. Rodríguez, Phys. Rev. Lett. **84**, 2199 (2000)

[40] A. Hernández-machado, J. Soriano, A. M. Lacasta, M. A. Rodríguez, L. Ramírez-Piscina,J. Ortín, Europhys. Lett. **55**, 194 (2001)

[41] David Jacqmin, J. Comp. Phys. **155**, 96 (1999)

[42] W. Villanuava and G. Amberg, Int. J. Multiphase Flow **32** 1072 (2006)

[43] P. Yuan, L. Schaefer, Phys. Fluids **18**, 042101 (2006)

[44] P. Papatzacos, Physica Scripta **61** 349 (2000)

[45] E. Zwaan, S. Le Gac, K. Tsuji and C.-D. Ohl, Phys. Rev. Letters **98** 254501 (2007)

[46] R. Teshigawara and A. Onuki, arXiv:1108.0213v1 (2011)

[47] T. Colonius, Annu. Rev. Fluid Mech. **36**, 315 (2004)

[48] J. H. Ferziger and M. Perić *Computational Methods for Fluid dynamics* 2nd ed. Springer (1999)

[49] H. T. Phan, N. Caney, P. Marty, S. Colasson and J. Gavillet, C. R. Mecanique **337**, 251 (2009)

[50] H.J. Palmer, J. Fluid Mech. **75**, 487 (1976)

Aalto-DD 141/2011

ISBN 978-952-60-4432-3
ISBN 978-952-60-4433-0 (pdf)
ISSN-L 1799-4934
ISSN 1799-4934
ISSN 1799-4942 (pdf)

Aalto University
Aalto School of Science
Department of Applied Physics
www.aalto.fi

BUSINESS + ECONOMY

ART + DESIGN + ARCHITECTURE

SCIENCE + TECHNOLOGY

CROSSOVER

DOCTORAL DISSERTATIONS